7-11-2017

Sodium Alginate Toughening of Gelatin Hydrogels and Elucidation of Possible Mechanisms

Michael Samp
sampma@rose-hulman.edu

Sodium Alginate Toughening of Gelatin Hydrogels and Elucidation of Possible Mechanisms

A Thesis

Submitted to the Faculty

Of

Rose-Hulman Institute of Technology

by

Michael Anthony Samp

In Partial Fulfillment of the Requirements for the Degree

of

Master of Science in Chemical Engineering

July 2017

ABSTRACT

Samp, Michael Anthony

M.S.Ch.E.

Rose-Hulman Institute of Technology

July 2017

Sodium Alginate Toughening of Gelatin Hydrogels and Elucidation of Possible Mechanisms

Thesis Advisors: Dr. Adam Nolte and Dr. David Henthorn

Hydrogels are soft materials used in several important biomedical applications such as drug delivery, wound dressing, tissue phantoms, and tissue engineering. Gelatin hydrogels, in particular, have several properties which would make them ideal materials, however, their poor mechanical and thermal properties often require enhancement to be viable. This report focuses on the addition of sodium alginate, another common biomacromolecule, to gelatin hydrogels and the resulting viscoelastic properties of these hybrid materials. Initial data collected using a parallel plate compression-to-failure testing setup suggested the hybrid samples had a larger toughness while showing a negligible change in the elastic modulus, an important parameter for biomimickry. Stress relaxation tests were performed in an attempt to characterize the linear viscoelastic properties of these materials along with thermogravimetric analysis (TGA) to elucidate the underlying mechanism responsible. Additional failure tests were conducted while varying pH to determine what effect, if any, electrostatic interactions between neighboring macromolecules, a common source of viscoelasticity, had on the overall mechanical properties. An additional set of failure tests was performed using a spherical indenter and confined sample

geometry in order to confirm the previously observed toughening effect while mitigating several sources of error inherent to the parallel plate test. These two experiments gave conflicting results regarding the bulk toughness of these samples. However, qualitative differences observed during these experiments, in conjunction with sessile drop contact angle measurements, may point towards a change in the surface characteristics, the hydrophilicity in particular, of these materials as a potential cause for the previously observed toughness enhancement.

Keywords: gelatin, alginate, hydrogel, toughness, modulus, mechanical properties, viscoelastic, modeling, relaxation

DEDICATION

For Taylor and my parents

ACKNOWLEDGEMENTS

I would like to thank my advisors, Dr. Adam J. Nolte and Dr. David B. Henthorn, for their guidance and support, as well as Dr. Mark E. Brandt for his expertise on collagen.

Thank you to Nicolae Iovanac for his assistance with much of the earlier parts of this work as well as Dr. Michael Insana and Yue Wang at UIUC for their advice and expertise in the field of gelatin tissue phantom engineering.

I would also like to thank the Rose-Hulman Departments of Chemical Engineering and Chemistry for their facilities and Mr. Frank Cunning and Mr. Lou Johnson for their assistance using said facilities.

Finally, thank you to the Rose-Hulman Department of Graduate Studies for funding for my studies and this project. Additional funding for this research was provided by the NSF under award number ECCS-1306808. This work is reproduced in part with permission from *ACS Biomaterials Science & Engineering*, submitted for publication. Unpublished work including portions of the text and Figure 6-9 are copyright 2017 American Chemical Society.

TABLE OF CONTENTS

LIST OF FIGURES

LIST OF ABBREVIATIONS

ATR FTIR	Attenuated Total Reflectance Fourier Transform Infrared Spectroscopy
DMA	Dynamic Mechanical Analysis
DSC	Differential Scanning Calorimetry
GM	Generalized Maxwell (model)
KVFD	Kelvin-Voigt Fractional Derivative (model)
MFD	Maxwell Fractional Derivative (model)
SSE	Sum of squared error
TGA	Thermogravimetric Analysis

LIST OF SYMBOLS

English symbols

E	Young's modulus
T_L	Level-off temperature
t	Time
t_R	Duration of ramp
G	Relaxation modulus
F	Force
R	Radius of indenter
d	Depth of indentation

Greek symbols

α	Order of fractional viscoelastic element
η	Viscosity of viscoelastic element
τ	Relaxation time constant
σ	Stress
ϵ	Strain
ν	Poisson's ratio

Mathematical symbols

$\mathcal{M}$	Mittag-Leffler function

1. INTRODUCTION

1.1 Gelatin/Alginate Structure, Applications, and Hydrogel Network Formation

Gelatin is a water-soluble biopolymer derived from the partial hydrolysis of collagen, the major structural protein in connective tissues.[1] Gelatin has been used as glue since around 4000 BC and today is widely used in the food, pharmaceutical, cosmetic, and photographic industries.[2-4] Gelatin is most commonly sourced from bovine or porcine skin or bone and is available in either Type A or Type B depending on whether the extraction conditions were acidic or alkaline, respectively.[3-5] The composition of gelatin can vary based on the source but, in general, the five most common amino acids are glycine (~30%), proline (~16%), hydroxyproline (~14%), glutamic acid (~12%), and alanine (~10%).[1, 3-5] The structures and pK_a values of these amino acids can be found in Figure 1.

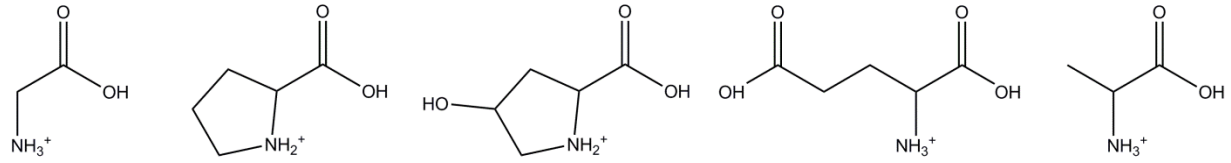

Figure 1. The five most common amino acids in gelatin and the associated pK_a values of the free amino acid.[6]

While these five amino acids are the main structural components of collagen (and therefore gelatin), they are not all relevant to the electrostatic interactions between neighboring gelatin chains. Since one carboxylic acid and one amine group are consumed in the formation of a peptide bond, only amino acids with side chains which can be protonated are important to these interactions assuming the chains are long enough that end groups can be ignored. Of these, the

most abundant in collagen are glutamic acid, arginine, aspartic acid, lysine, and histidine. The structures and side-chain pK_a values of these amino acids can be found in Figure 2.

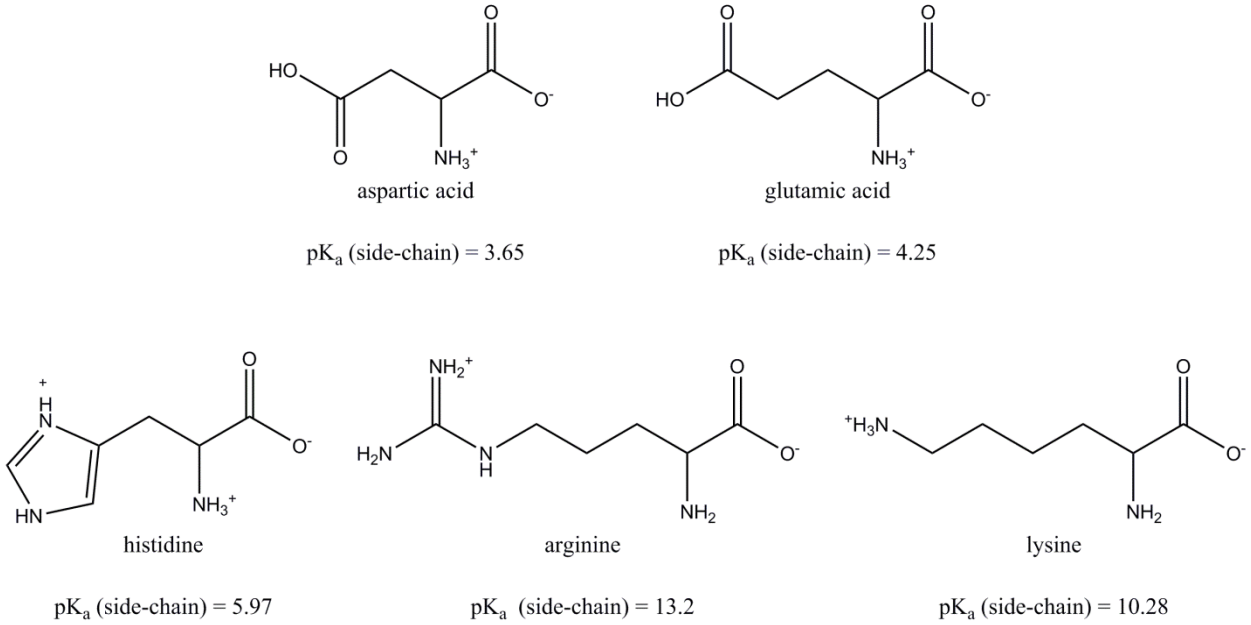

Figure 2. Chemical structures and side-chain pK_a values of the amino acids relevant to electrostatic interactions between gelatin chains.

The structure of collagen is defined by three α chains which come together to form a single, stable right-handed collagen helix.[5] This collagen helix is stabilized by intra- and intermolecular hydrogen bonds between α chains. During the gelatin extraction process, the collagen helices are denaturated during the heating step and partially reform during cooling.[5] A similar process governs the formation of a thermoreversible gelatin network. When gelatin is dispersed in warm water, the intermolecular hydrogen bonds between α chains are broken and random coil polymers are formed in solution. Upon cooling, they re-associate, trapping water within the structure. Owing to the many hydrophilic groups in the gelatin structure, water can occupy several positions within the hydrogel matrix including the formation of hydrogen bonds between two neighboring α chains. Since an individual α chain can form hydrogen bonds either through intermolecular interactions or by folding back on itself, there is a minimum

concentration (~0.5% w/w) necessary to form a complete 3D network. Below this concentration, intramolecular associations dominate and prevent the formation of a network.

Relatively soft gelatin hydrogels (< ~8% w/w) suffer from poor mechanical properties. As an example, these materials are quite brittle and simply handling them can cause fracture or surface defects. This makes these materials difficult to work with and can limit their applications, especially if a pristine surface is required. The mechanical properties of gelatin are often improved by the addition of a crosslinking agent such as glutaraldehyde, genipin, or 1-ethyl-3-(3-dimethylaminopropyl) carboiimide (EDC).[7-10] However, the addition of a crosslinking agent inherently changes the nature of the gel network. By forming covalent bonds between gelatin chains, the resulting structure is a permanent chemical gel, rather than the standard, thermoreversible physical network. Modification can also be made by including any number of additives in the formulation. Common examples include plasticizing molecules such as glycerol or a second macromolecule such as sodium alginate or gum arabic.[9, 11, 12]

Sodium alginate (or the acid form, alginic acid) is a polysaccharide, produced commercially through extraction from algae or seaweed, consisting of β-D-mannuronate (M) and α-L-guluronate (G) residues linked 1 → 4 in a linear, random copolymer (Figure 3).[13] Like gelatin, sodium alginate has the ability to form a hydrogel, although it can do so by two different methods. The first is to lower the pH of an alginate solution below the pK_a values of the individual uronic acid residues, which have been found to be 3.38 and 3.65 in 0.1 M NaCl for mannuronic acid and guluronic acid, respectively.[14] When $pH < pK_a$, the carboxylate groups become protonated and intermolecular hydrogen bonds form an acid gel network. The second method to form a hydrogel from sodium alginate is by the addition of divalent cations to form

what is known as an "ionotropic hydrogel".[15] A number of different divalent ions can be used, but calcium salts are used most commonly (*e.g.*, $CaCl_2$, $CaSO_4$).[16-18]

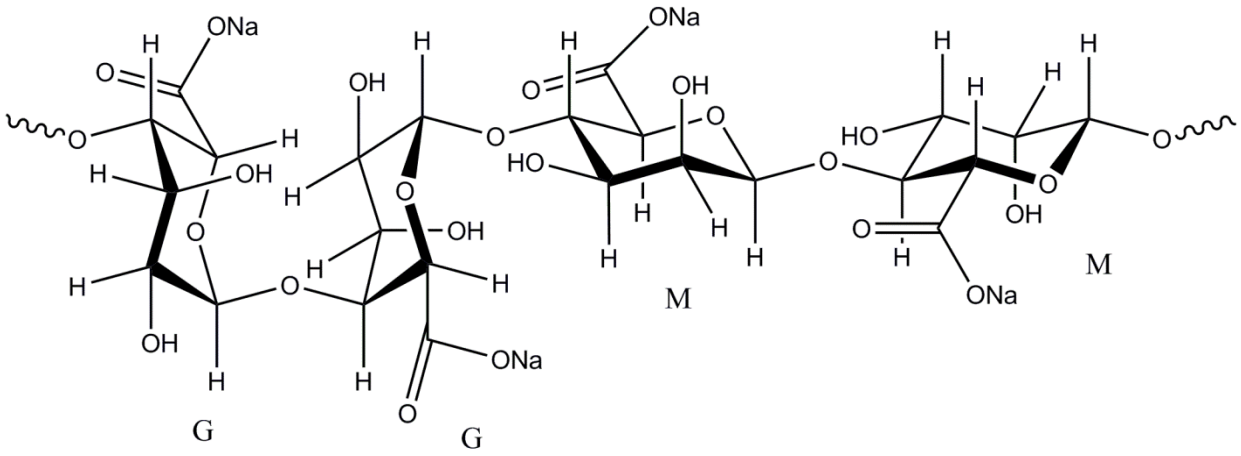

Figure 3. Structure of sodium alginate consisting of $\boldsymbol{\alpha}$-L-guluronate (G) and $\boldsymbol{\beta}$-D-mannuronate (M) residues.

The prevailing theory for the mechanism behind calcium alginate gelation is the formation of "egg-box" junctions between two neighboring alginate molecules.[17, 19] From Figure 3 it is clear the M and G residues have different spatial conformations. M residues form flat, ribbon-like structures whereas G residues have a buckled structure. When Ca^{2+} ions are present in solution, this conformational difference allows the carboxylate groups of G residues to bind more strongly to the Ca^{2+} ion than the M carboxylates. Nearby alginate molecules can form "pockets" with their G residues, and upon addition of calcium ions, the ion will fill in this pocket and the two molecules will be bound by chelation. Due to the spatial arrangement of polymannuronate, it is unable to perform this same mechanism. It follows that the strength of alginate gels should depend both on the molecular weight of the polymer as well as the ratio of mannuronate residues to guluronate residues, with high-MW alginates high in guluronate being stronger due to increased interchain interactions.[19] However, it should be noted that for larger divalent cations (*e.g.*, Co, Cu, Mn) gelation does not occur by the formation of egg-box junctions

and the M/G ratio is of lesser importance.[17] The M/G ratio is typically measured by ^{1}H-NMR with a procedure proposed by Grasdalen.[20, 21]

These macromolecules have the advantage of being cheap, easy to use, safe, and have excellent biocompatibility which make them ideal candidates for biomedical applications such as wound dressing, drug delivery, and tissue phantoms or scaffolds.[15, 22-28] An additional characteristic that makes gelatin and alginate ideal biomaterials for tissue phantom/engineering purposes is the ease with which their mechanical properties can be tuned. This quality's importance for creating biologically-accurate tissue phantoms is obvious when it comes to preparing durable samples that accurately replicate the stiffness and viscoelastic properties of biological tissues. Mechanical properties can also be important in tissue engineering applications for controlling cell attachment and proliferation.[10, 23] The mechanical properties of gelatin/alginate blend films have been studied previously for wound dressing and drug delivery applications, however, very little research has been done into the mechanical properties of highly hydrated, three-dimensional blends of these macromolecules which may be useful biomaterials for low-cost tissue phantoms.[9, 11, 29]

In particular, gelatin-polysaccharide gels have been of interest in recent decades. Blends of gelatin with various polysaccharides such as alginate, chitosan, gum arabic, and pectin have been studied.[12, 30-32] The mixture of two separate biopolymers creates an extremely complex system in which attractive and repulsive interactions between macromolecules are governed by a number of different factors including pH, ionic strength, protein-to-polysaccharide ratio, molecular weight, and many others. Especially of interest is the formation of protein-polysaccharide complexes by attractive electrostatic interactions between the oppositely charged macromolecules. Depending on the pH and ionic strength of the surrounding environment, these

complexes can potentially cause liquid-liquid phase separation (referred to as complex coacervation) or liquid-solid phase separation (referred to as precipitation). The formation of protein-polysaccharide complexes may also have an effect on the mechanical properties of these blend hydrogels by interrupting the partial renaturation of triple helices, increasing chain entanglements, or moderating interactions between gelatin chains.

1.2 Viscoelastic modeling

Hydrogels are interesting materials because often they have significant viscoelastic characteristics which give them mechanical properties between a liquid and a solid. Covalent bonds in the backbones of gelatin and alginate provide rigidity to the overall structure, responding elastically to small changes in strain. The hydrogel network also contains a significant number of hydrogen bonding and electrostatic interactions which can easily break and reform allowing the material to relax when a stress is applied and giving it some liquid-like character.[27]

These viscoelastic properties can be studied by a number of different ways including dynamic mechanical analysis (DMA), rheometric analysis, ultrasound elastography, or quasi-static compression or tensile tests.[9, 10, 26-28, 33-35] Quasi-static compression tests will be used throughout this report. Using quasi-static compression, the most common way to measure viscoelastic properties is to apply a force to the sample and observe the sample's stress relaxation, fitting the data to a viscoelastic model. The viscoelastic models to be used in this report are shown in Figure 4.

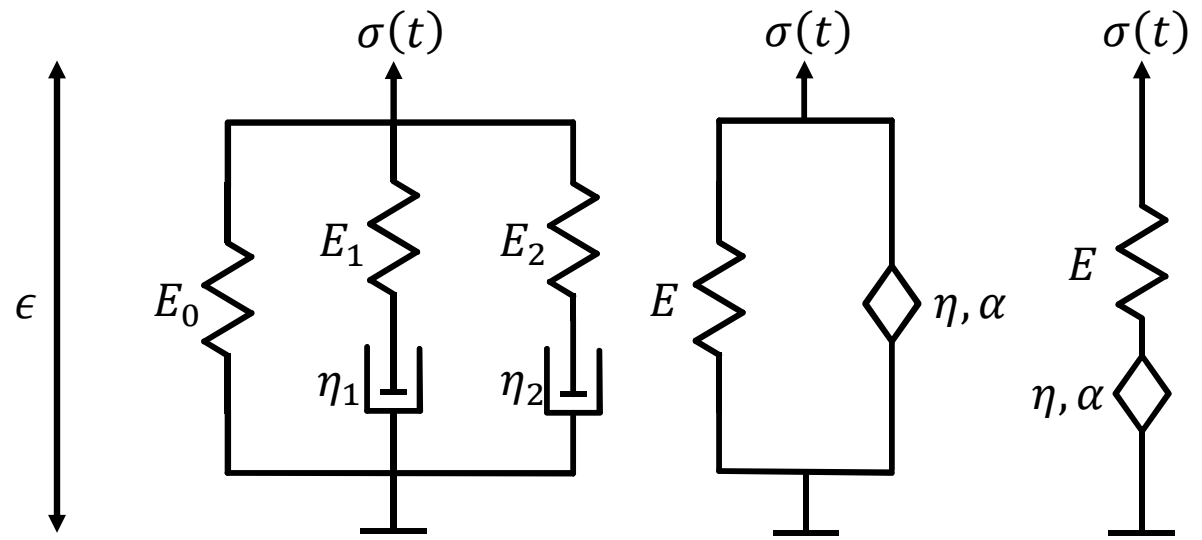

Figure 4. (From left to right) The Generalized Maxwell (GM), Kelvin-Voigt Fractional Derivative (KVFD), and Maxwell Fractional Derivative (MFD) viscoelastic models. Springs represent an elastic response (***E***), dashpots represent a viscous response (***η***), and diamonds represent fractional-order viscoelastic elements (***η***,***α***).

The representations of these viscoelastic models are quite similar to electrical circuits, with combinations of springs and dashpots in series and parallel. Springs are Hookean elements which obey the relationship,[36]

$$\sigma = E\epsilon \tag{1}$$

and dashpots are Newtonian elements which obey the relationship,[36]

$$\sigma = \eta \frac{d\epsilon}{dt} \tag{2}$$

where σ is the stress on the element, E is the modulus of the element, η is the viscosity of the element, and ϵ is the strain on the sample.

The Generalized Maxwell (GM) model (Figure 4, left) is one of the simplest viscoelastic models and consists of a Hookean element in parallel with a number of "Maxwell arms" which are a Hookean and Newtonian element in series. These Maxwell arms can be used to model stress relaxation which occurs on multiple time scales within the material, with each one contributing a single time constant. Throughout this report the naming convention used for

different GM models will be the letters "GM" followed by the number of fitting parameters in the model. For example, the GM model in Figure 4 has two Maxwell arms, each contributing two parameters, so it would be named GM-5.

The other two viscoelastic models used to fit stress relaxation data in this report are the Kelvin-Voigt Fractional Derivative (KVFD) (Figure 4, center) and the Maxwell Fractional Derivative (MFD) (Figure 4, right) models. One obvious different between these two models and the GM model is that the Newtonian element has been replaced with a new element, represented by a diamond, which makes use of a mathematical operation known as a fractional derivative and obeys the relationship,[37]

$$\sigma = \eta \frac{d^{\alpha}\epsilon}{dt^{\alpha}} \tag{3}$$

where α is the order of the derivative, which for this application will take on values between zero and one. By introducing a new time constant, τ, for the fractional-order element by $\eta = E\tau^{\alpha}$, Equation 3 can be re-written as:[35, 37]

$$\sigma = E\tau^{\alpha} \frac{d^{\alpha}\epsilon}{dt^{\alpha}} \tag{4}$$

Note that when the value of α is zero Equation 4 simplifies down to Equation 1, indicating a purely elastic (Hookean) response. Also, when the value of α is one Equation 4 simplifies to Equation 2, indicating a purely viscous (Newtonian) response. Therefore, a single fractional-order element (Equation 4) is able to represent a distribution of relaxation times for viscoelastic materials. Specifically, these fractional calculus models are power laws in time and have been shown to be able to model relaxation over several decades of time scale.[36-38]

To analyze a material's viscoelastic response via quasi-static compression, the sample is strained and the observed stress response is compared to the response predicted by each

viscoelastic model. The theoretical stress response for any model can be calculated for a given strain profile by the Boltzmann superposition integral:

$$\sigma(t) = \int_0^t G(t-t')\frac{d\epsilon}{dt'}dt' \tag{5}$$

where $G(t)$ is the relaxation modulus for a particular model, which is equivalent to the model's predicted stress response to a Heaviside step-strain function (an instantaneous change in strain at t = 0).[39] Due to practical difficulties in producing a repeatable step change in strain, a ramp-hold function is often used instead, where:[35]

$$\epsilon(t) = \begin{cases} \frac{\epsilon_0}{t_R}t, & t < t_R \\ \epsilon_0, & t \geq t_R \end{cases} \tag{6}$$

where ϵ_0 is the strain at the end of the ramp and t_R is the duration of the ramp. Other researchers have previously derived expressions for the relaxation modulus for each of the models studied.[35, 37, 40] Once a theoretical stress response has been calculated, it can be compared to the experimental stress response and the model parameters can be determined by minimizing the sum of squared error (SSE), which will be described in later sections.

2. MATERIALS AND METHODS

2.1 Materials

Gelatin powder, 250 Bloom Type B, was obtained from Custom Collagen (Addison, IL). The isoelectric point and molecular weight distribution were not experimentally determined, but typical values for this type of gelatin are pH 4.7 – 5.2 and 60 kDa, respectively.[3, 4, 41] Sodium alginate, extracted from seaweed, was purchased from Sigma-Aldrich. The molecular weight of this product is estimated to be between 120,000 – 190,000 g/mol and the M/G ratio (ratio of

mannuronic acid residues to guluronic acid residues) is approximately 1.56.[42] Ultrapure (Type 1) deionized (DI) water was obtained from a Direct-Q® 3UV water purification system.

2.2 Sample Preparation

Gelatin powder was mixed with DI water at room temperature and heated in a 68°C water bath for one hour, stirred every five minutes. Next, the pH was adjusted with either 1.0 M HCl or 1.0 M NaOH and make-up water was added to achieve the desired final gelatin (5% w/w) and alginate concentrations. For the remainder of this report, the reported gelatin and alginate concentrations are taken at this point and evaporative losses that occur from this point forward in the sample preparation are not considered. Following the pH adjustment, sodium alginate is added and the solution is stirred vigorously, covered, for 30 minutes or until the solution is homogeneous, whichever is longer. The maximum time given for the dissolution of the alginate was 45 minutes. Beyond this, the gelatin solution would cool and begin to gel, becoming too viscous to work with. The pH adjustment and the addition of alginate were performed in this order to prevent the precipitation of alginic acid, which can occur when the pH of the solution drops below the pKa of the uronic acid residues (3.38 and 3.65 for mannuronic and guluronic acid, respectively).[14] The pH of the homogeneous solution was measured with a VWR sympHony combination pH probe with temperature sensor (89231-608) using a VWR sympHony H10P handheld pH meter. By the time the pH measurement was taken, the solution had cooled to 30-35^{o}C.

The method of storage was dependent on the test the sample was to be used for. Samples to be used for parallel-plate compression tests were poured, to a mass of 20 g, into cylindrical PVC molds (inner diameter = 35 mm) which had been sprayed with mold release spray (MR 311 by Sprayon). The final sample heights were approximately 21 mm. The molds were then sealed

with parafilm to minimize evaporative losses and stored at room temperature for 24 hours. The same procedure was used for spherical puncture tests; however, the molds were filled to a mass of 30 g to minimize the effects of the bottom plate during the test. Samples to be lyophilized or used for TGA were poured into a polystyrene Petri dish, sealed with parafilm, and stored at room temperature for 24 hours. Finally, samples to be used for ATR-FTIR were pipetted onto a glass microscope slide which had been washed thrice with DI water. These slides were then allowed to set and dry on the lab bench for 24 hours in order to form a film.

2.3 Unconfined, parallel plate compression tests

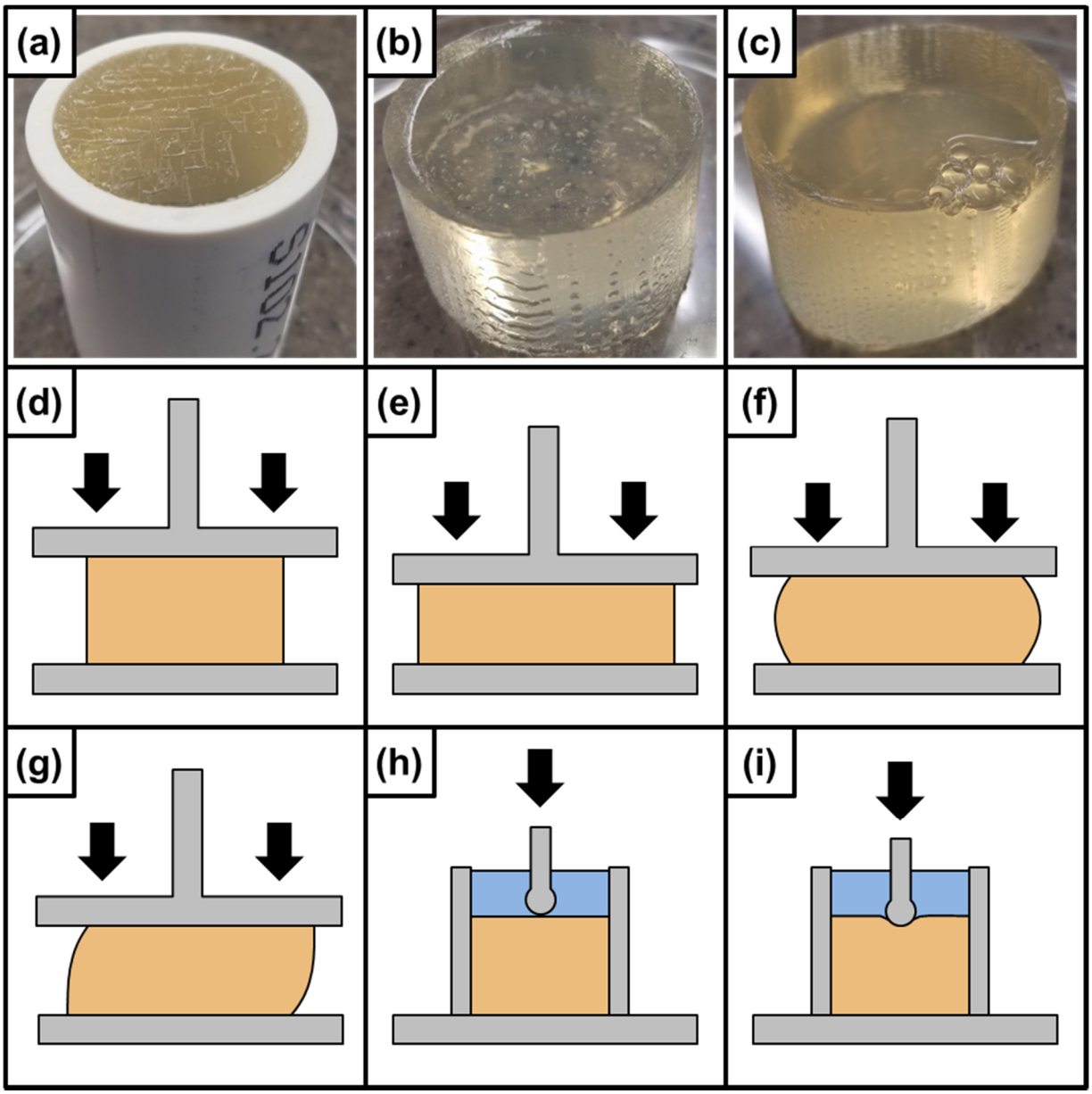

Figure 5. Sources of possible error during parallel plate compression-to-failure testing and the alterative testing method. (a) peeling at top surface due to parafilm removal, (b) "pitting" on sides of a sample, (c) bubbles on bottom surface, (d) cartoon of uncompressed sample, (e) cartoon of slip boundary condition, (f) bulging due to inadequate lubrication, (g) leaning due to off-center application of force or sample slumping, (h) and (i) spherical indentation method

All mechanical tests were performed with a Shimadzu EZ-SX Texture Analyzer equipped with a 200 N load cell. Samples were removed from the mold using a plunger-type device and their exact measurements were taken immediately prior to testing. All unconfined mechanical

tests were performed using a cylindrical aluminum testing head 10 cm in diameter. Prior to testing, both the bottom plate and the top surface of the sample were covered with water to facilitate free-slip conditions at both interfaces.

Due to the poor mechanical properties and brittleness mentioned earlier, the de-molding procedure often resulted in surface defects. These included peeling at the top face of the sample occurring during parafilm removal (Figure 5a), pitting on the outer surface caused by adhesion with the PVC mold during removal (Figure 5b), and air pockets on the bottom face caused by bubbles being trapped during gelation (Figure 5c). This final defect only occurred when the solution cooled too much before being poured, which happened most often with blend samples at low pH due to additional time being needed to dissolve the sodium alginate. These flaws are especially problematic when measuring ultimate compressive properties since they can potentially provide a location for an initial crack to form as a result of an increase in local stress. Once these cracks form, the entire sample can quickly become compromised and fail prematurely, resulting in a lower than expected toughness.

In an ideal unconfined, parallel plate compression-to-failure experiment, both sample/plate interfaces would be frictionless and the sample would expand evenly in the radial direction (Figure 5d,e). However, inadequate lubrication at the sample/plate interfaces or an off-center application of force may cause the sample to bulge in the middle or lean to one side during testing (Figure 5f,g). Both of these non-ideal deformations result in uneven loading which can create a localized increase in stress in the same way as the surface defects. These asymmetries are accentuated at larger strains. Since every sample exhibited bulging to some extent, a visual assessment was performed during each test to determine if the data collected were reliable.

In order to determine the initial point of contact with the sample, the testing head was placed just above the top surface of the sample and was brought down slowly (0.02 – 0.05 mm s^{-1}) until a force of 0.05 N was read, which corresponds to approximately 2% strain. The testing head was then raised at the same rate until a reading of 0 N was achieved. The purpose of this procedure was to ensure the entire face of the sample was in contact with the testing head to negate any effects of the small (< 1 mm) meniscus which formed as a result of the casting procedure.

From this point, two different types of test were performed: compression-to-failure or ramp-hold force relaxation. In the compression-to-failure tests, samples were compressed at a strain rate of 0.5 % s^{-1} until failure was observed. One confounding factor in performing this test is the lack of a clear point of failure in some cases. In some instances, when the sample breaks it does not slide out from under the testing head and continues to be compressed, which can obfuscate the actual failure point in the resulting stress-strain curve. In cases where this occurred, the point of failure was determined either by visual inspection or by the point where the observed stress deviated from its normal upward trend. The toughness of a sample was calculated by integrating the area under the stress-strain curve up to the failure point. The elastic modulus of the sample was determined by performing a linear least-squares regression on the stress-strain curve between 0.5% and 3% strain, and the strain-to-break was determined as the strain at which the failure point occurred.

Two different ramp-hold stress relaxation tests were performed. The first was run at lower overall strains (5%), with a strain rate of 0.5 % s^{-1}, followed by a five-minute holding period. The second set of experiments was run at a higher overall strain (25%) and was compressed much more quickly (5 % s^{-1}), followed by the same five-minute holding period.

2.4 Confined spherical puncture tests

A series of puncture tests (Figure 5h,i) where the samples were left in their molds were also performed. Due to the mold's opacity, sample dimensions and the initial point of the contact were determined as follows. First, an object with a known height was used to zero the stroke reading of the instrument. Next, the top surface of the sample was covered with water to minimize adhesive forces between the sample and the indenter. The sample was then compressed with a spherical aluminum indenter (diameter = 7.93 mm) at a rate of 0.05 mm s^{-1} until a force of 0.02 N was read. The indenter was then raised until a reading of 0 N was achieved. The height of the sample was then taken as the known height of the object used earlier minus the distance the testing head had moved during this procedure. Sample heights used for this test averaged around 30 mm. Once the initial point of contact and sample height had been determined, the sample was indented at a rate of 0.5 % s^{-1} until failure was observed. Unlike the unconfined compression-to-failure tests described earlier, these puncture tests had a very clear point of failure.

The goal of the confined puncture test is to provide a second measurement of the material's ultimate compressive strength while mitigating the many sources of error associated with the de-molding procedure and inadequate lubrication as discussed earlier. It was assumed that the underlying mechanism governing the ultimate failure properties of these materials would behave similarly in each experiment, allowing a qualitative comparison between the two. Furthermore, by eliminating several sources of experimental error it may to gain additional insight into the origin of this mechanism.

2.5 Thermogravimetric analysis (TGA)

TGA measurements were taken with a TA Instruments TGA Q50 Series. Samples to be analyzed were excised by hand from Petri dishes which had been cured at room temperature for

24 hours. Samples were roughly cubic and had an initial mass of approximately 15-40 mg. Samples were placed in an aluminum pan which was placed on the platinum sample holder. The flow rate of nitrogen in the balance was 40 mL min^{-1} and 60 mL min^{-1} in the sample chamber. Tests were run in ramp mode at a heating rate of either $10^{o}C\ min^{-1}$ or $1^{o}C\ min^{-1}$ from room temperature up to a maximum temperature of $500^{o}C$. Since the relevant region of the thermogravimetric curve was only the area where water was lost, for the sake of time, the tests run at $1^{o}C\ min^{-1}$ were stopped once the thermogravimetric curve had leveled off following water loss.

2.6 Attenuated Total Reflectance Fourier Transformed Infrared Spectroscopy (ATR-FTIR)

IR measurements were taken with a Shimadzu IRPrestige-21 and spectra were analyzed with IRSolution software. The ATR cell was an AccessATR™ Single Reflection ATR accessory with a ZnSe crystal from Harrick Scientific Products. Prior to each test, the crystal was cleaned with isopropyl alcohol and given a few minutes to allow the solvent to evaporate. The sample films, described earlier, were then firmly pressed into the crystal using the attached screw. IR measurements were taken with an air background for 64 scans with 2 cm^{-1} resolution over 600-4000 cm^{-1}.

2.7 Contact angle measurements

Water droplets (approximately 7.7 μL) were dropped onto freshly prepared, fully-hydrated surfaces. Contact angle measurements were made in air with a Krüss FM40 EasyDrop goniometer and contact angles and drop volumes were calculated using the Drop Shape Analysis software package, assuming a sessile drop.

2.8 Ramp-hold stress relaxation modeling

All modeling was done in MATLAB by varying a given model's parameters to minimize the sum of the squared errors between experimental data and the model fit. Due to random noise in the force reading, the force was not always zero when data collection began. Before running the fitting algorithm, all data was shifted up or down such that the first point was equal to zero. The magnitude of this shift was never more than ± 0.002 N.

Due to the coupled nature of the E and τ parameters in the KVFD and MFD models, these parameters are very sensitive to the initial values supplied to the algorithm. The initial value for τ was always set to 150 s (approximately half of the total testing time). The parameters E and α were varied manually to approximate the fit, and these approximations were supplied to the algorithm as the initial values for the parameters.

The experimental data was also fit with the GM model, which contains pure Newtonian dashpot elements, rather than the fractional forms present in the previously described models. A GM model with one Maxwell arm (GM-3) is more commonly known as the Standard Linear Solid or Zener model. Finally, the data was also fit with a GM model containing two Maxwell arms (GM-5). This latter model was used to observe the relative advantage that could be gained by allowing more fitting parameters (five, as opposed to the three parameters each of the other models contain) into a standard linear viscoelastic model.

It should be noted that a different technique was necessary when modeling the data taken from the high strain experiments. At the strain at which these tests were performed the samples no longer displayed a linear stress response in the ramp region, which made fitting the entire ramp-hold stress responses difficult. Instead, a relatively fast ramp was used to approximate a step change in strain, and the holding period was modeled with a five-term Prony series, which

represents a GM-5 model response following a step change in strain. In order to get more accurate fits in the region immediately following the ramp, this model was constrained to pass through the first experimental data point of the holding region.

3. RESULTS AND DISCUSSION

3.1 Effect of alginate concentration on mechanical properties

The first objective was to quantify the effect of sodium alginate concentration on the mechanical properties of the gelatin samples. Figure 6 summarizes the effect alginate concentration has on the three main mechanical properties to be studied in this report: Young's modulus, toughness, and strain-to-break. All values discussed in this section were determined by an unconfined, parallel-plate compression-to-failure test.

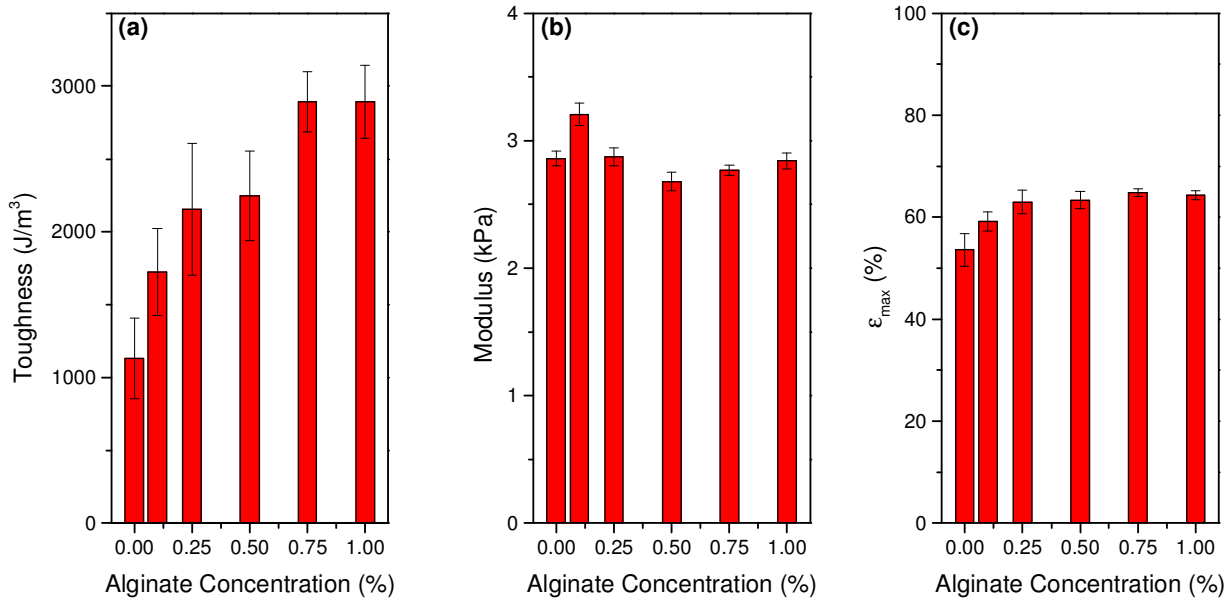

Figure 6. Plots of (a) toughness, (b) elastic modulus, and (c) strain-to-break as a function of alginate concentration. The height of each bar represents the average of all trials and the uncertainty bars represent the standard error in the average measurement. For these results, seven samples were tested at each alginate concentration.

Figure 6a shows that, in general, toughness increases with increasing alginate concentration. The addition of just 0.1% w/w alginate increased the measured toughness by 52%, and adding more than 0.75% increased the toughness by approximately 150%. During testing, it was necessary to use two separate batches of gelatin powder. In the first batch, the observed toughness increase was larger (a 120% increase at 0.1% w/w and 480% increase at 0.75%), than in the second batch (a 58% increase at 0.1% w/w and a 78% increase at 0.75%). In the second batch of gelatin, however, the "neat" gelatins samples (with no alginate) were naturally tougher (the average toughness of the neat samples in the first batch was 511 J/m^3, while the average toughness of the neat samples in the second was 1598 J/m^3). Because gelatin is a natural product, slight variations in mechanical properties between batches of the same product are to be expected, but no additional characterization was performed to determine if differences in molecular weight or ion content were present. For each batch, however, a relative increase in toughness was observed upon addition of alginate. Figure 6 shows the averages of all data across both batches.

Toughness is calculated by integrating the area under the force-displacement curve up to the point of failure; generally speaking, it can be increased by either increasing the elastic modulus (more force required to achieve the same level of strain), or by increasing the strain-to-break of the material. Because the Young's modulus of tissue phantoms is often a key parameter in accurately mimicking biological tissue of a specific stiffness, it is desirable to increase the toughness without changing the modulus of the material (i.e. increase strain-to-break).

Figure 6b shows that for the range of alginate concentrations tested, the average elastic modulus at each concentration remained relatively constant, varying between approximately 2.8 and 3.2 kPa. There is an apparent spike in the Young's modulus from 2.86 kPa at 0% w/w

alginate to 3.21 kPa at 0.1% alginate. This peak was found to be statistically significant ($p = 0.006$), however, a second set of trials run with the same conditions and using the same method did not contain this peak. A rise in modulus at low alginate concentrations could be possible as a result of alginate scavenging Ca^{2+} ions (which act as ionic crosslinkers) from the gelatin matrix and forming either a biphasic fluid phase within the gelatin matrix or possibly even an interpenetrating alginate matrix. These possibilities are discussed at length in Appendix B. At larger alginate concentrations, this effect would not be observed because there would not be enough Ca^{2+} ions in the gelatin to crosslink further alginate molecules to an appreciable degree. At any rate, even if a slight rise in Young's modulus exists at 0.1 % w/w alginate, the upward trend does not continue at higher alginate concentrations, and the modulus remains unchanged within statistical certainty up to 1.0% w/w alginate addition. Changes in the modulus do not therefore provide an explanation for the observed increase in toughness.

Instead, increases in the material's strain-to-break (Figure 6c) can be identified as the cause of the observed toughness increase. Adding only 0.1% w/w of sodium alginate increased the average strain-to-break from 53.6% to 59.2%, and adding 0.5% w/w or more of alginate increases the average failure strain to approximately 64%.

Qualitatively, gelatin/alginate samples were easier to de-mold and handle without fracture than their neat counterparts, which could be a key advantage for such materials in medical testing or training scenarios. It is important to note that when performing toughness experiments, any crack in the sample will create a localized stress increase that could lead to premature fracture. Therefore, only samples with no major surface defects were used. The potential problems caused by these defects as well as an alternative testing method to mitigate them will be discussed in a later section.

3.2 Modeling of ramp-hold stress relaxation

After quantifying the toughness enhancement imparted by alginate addition to gelatin samples, the next goal was to determine whether these improvements were reflected in the linear viscoelastic properties of the material. As described previously in the methods section, stress relaxation experiments were conducted using a ramp-hold strain profile, and the experimental results were modeled using Equation 5 above. For each of the models being studied, a form of the relaxation modulus, $G(t)$, has been found previously. For the GM model:[35]

$$G_{GM}(t) = E_0 + \sum_{i=1}^{k} E_i \cdot \exp\left(-\frac{t}{\tau_i}\right) \tag{7}$$

For the KVFD model:[35]

$$G_{KVFD}(t) = E \cdot \left(1 + \frac{\left(\frac{t}{\tau}\right)^{-\alpha}}{\Gamma(1-\alpha)}\right) \tag{8}$$

For the MFD model,[40]

$$G_{MFD}(t) = E \cdot \mathcal{M}_{\alpha}\left(-\left(\frac{t}{\tau}\right)^{\alpha}\right) \tag{9}$$

where $\mathcal{M}_{\alpha}$ is the Mittag-Lefler function defined by:[40]

$$\mathcal{M}_{\alpha,\beta}(z) = \sum_{k=0}^{\infty} \frac{z^k}{\Gamma(\alpha k + \beta)} \tag{10}$$

General nomenclature for the Mittag-Leffler function states that if the function only has one subscript, the value of β in the function is equal to one, i.e. $\mathcal{M}_{\alpha}(z) \equiv \mathcal{M}_{\alpha,1}(z)$. In this report, $\mathcal{M}$ is being used for the Mittag-Leffler function rather than the more common E, in order to avoid confusion with the Young's modulus.

Taking any of these forms of the relaxation modulus and plugging them into the Boltzmann superposition integral (Equation 5) yields a closed-form solution for the predicted stress response. For the GM model:

$$\sigma_{GM}(t) = \begin{cases} \dfrac{\epsilon_0}{t_R}\left(E_0 t + \displaystyle\sum_{n=1}^{k} E_n\tau_n\left(1-\exp\left(-\frac{t}{\tau_n}\right)\right)\right), & t \le t_R \\ \epsilon_0 E_0 + \displaystyle\sum_{n=1}^{k}\frac{E_n\tau_n}{t_R}\left(\exp\left(-\frac{(t-t_R)}{\tau_n}\right)-\exp\left(-\frac{t}{\tau_n}\right)\right), & t > t_R \end{cases} \tag{11}$$

For the KVFD model:

$$\sigma_{KVFD}(t) = \begin{cases} \dfrac{E\epsilon_0 t}{t_R}\left(1+\dfrac{\left(\frac{t}{\tau}\right)^{-\alpha}}{\Gamma(2-\alpha)}\right), & t \le t_R \\ \dfrac{E\epsilon_0}{t_R}\left(t_R - \dfrac{(t-t_R)\left(\frac{t-t_R}{\tau}\right)^{-\alpha}}{\Gamma(2-\alpha)} + t\dfrac{\left(\frac{t}{\tau}\right)^{-\alpha}}{\Gamma(2-\alpha)}\right), & t > t_R \end{cases} \tag{12}$$

For the MFD model:

$$\sigma_{MFD}(t) = \begin{cases} \dfrac{E\epsilon_0 t}{t_R}\mathcal{M}_{\alpha,2}\left(-\left(\frac{t}{\tau}\right)^{\alpha}\right), & t \le t_R \\ \dfrac{E\epsilon_0 t}{t_R}\mathcal{M}_{\alpha,2}\left(-\left(\frac{t}{\tau}\right)^{\alpha}\right) - \dfrac{E\epsilon_0}{t_R}(t-t_R)\mathcal{M}_{\alpha,2}\left(-\left(\frac{t-t_R}{\tau}\right)^{\alpha}\right), & t > t_R \end{cases} \tag{13}$$

Since the GM-3, KVFD, and MFD models each have three fitting parameters, a direct comparison was performed on these three models to determine their relative effectiveness at fitting a given set of stress relaxation data. Predicted stress data was generated using Equations 11-13 and Figure 7 shows an example of the model fits for a single data set. All three models do a reasonable job of fitting the long-term relaxation behavior of the samples (Figures 7a, b, and c). The two fractional models, however, do a much better job of fitting the region of the data immediately following the ramp (inset of Figures 7a, b, and c), which results in a much lower

overall SSE. This indicates that three parameter fractional element models have a greater ability to model the ramp-hold stress relaxation in these systems.

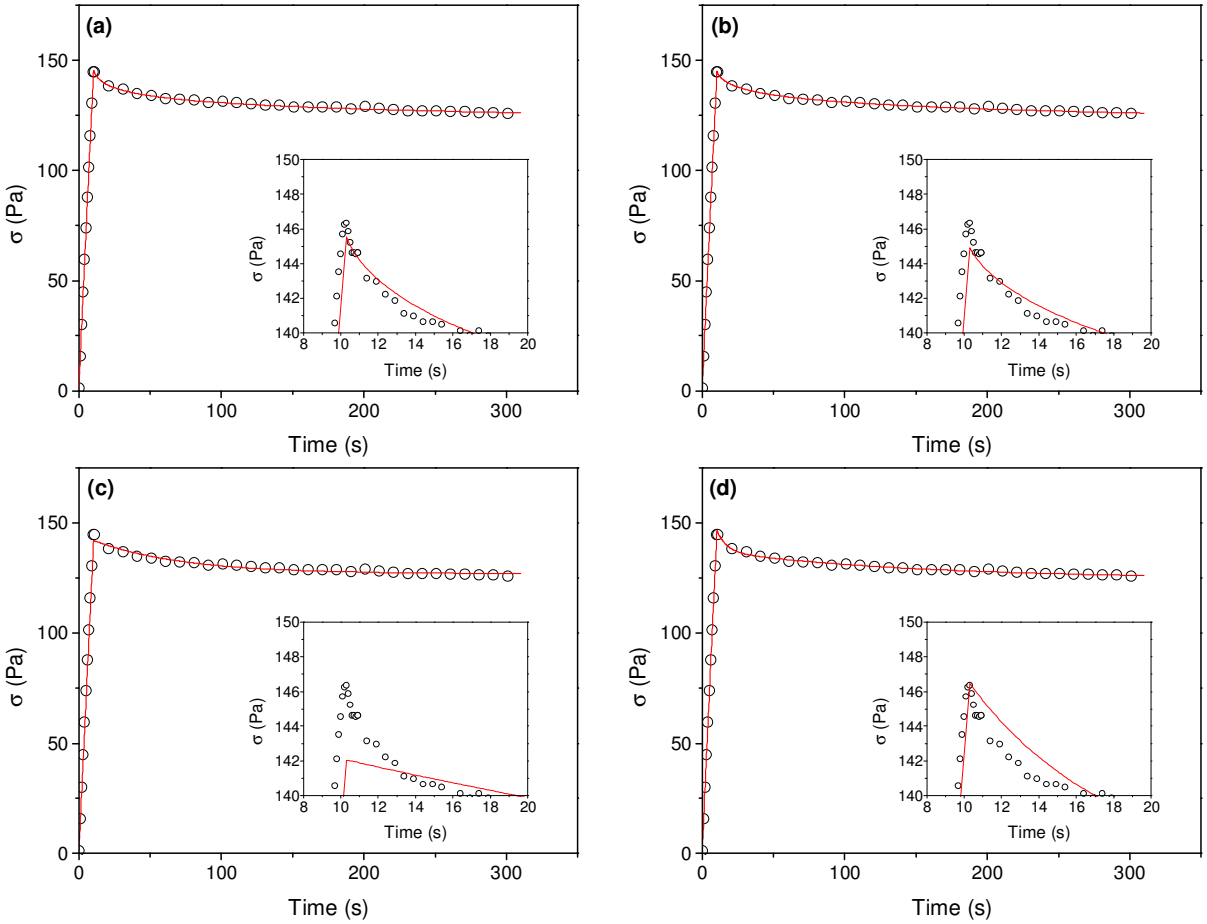

Figure 7. Model fits of a single data set using the (a) KVFD, (b) MFD, (c) GM-3, and (d) GM-5 models. Inset images are zoomed in on the end of the ramp portion of the data. Data in plots are downsampled by a factor of 10 in the ramp region and 100 in the hold region for visualization purposes.

The ability of three-parameter fractional calculus models to better fit the stress relaxation data suggests that stress relaxation in gelatin-based hydrogel systems benefit from the flexibility of models with a tunable degree of viscoelastic character, reflected here in the parameter α. Gelatin samples, in particular, comprise a random network of hydrogen-bonded crosslinks. The addition of sodium alginate, which may be electrostatically crosslinked through the presence of residual divalent cations in the gelatin, would presumably yield an interpenetrating or biphasic

network structure capable of viscous relaxations over a spectrum of time scales, as has similarly been observed in other polymeric systems.[43] Viscous dissipation could also occur due to physical entanglements between gelatin and alginate chains or electrostatic interactions between these chains which could quickly break and re-form.

Given these considerations, it is no surprise that the GM-3 model, which predicts an exponential stress relaxation with a single time constant, $\tau = \eta/E$, provided a comparably worse fit for the experimental stress relaxation data (Figure 7c). Adding additional "arms" to the GM model can provide a better fit for the data through the inclusion of additional parameters (each arm adds another Young's modulus and viscosity term, and hence another relaxation time parameter). Figure 7d shows the model fit when using a GM-5 model. Despite a comparable SSE between this five-parameter GM-5 model and the two three-parameter fractional models, the inset image reveals that the GM-5 model still underestimate the amount of relaxation happening on small time scales (a trend that was usually true across multiple samples), again suggesting the superiority of the fractional models for capturing dynamic stress relaxation in the gelatin material.

Despite observed success of the fractional models in modeling stress relaxation in gelatin and gelatin/alginate samples, the computational fitting routines were not straightforward to implement. Without careful selection of starting parameters, the fitting algorithms could converge to widely different sets of parameter values with a similar overall SSE. Care must be taken to avoid local minima traps and solutions with unrealistic values (typically very large or small values of E or τ). Some consistency was gained by initially adjusting the fitting parameters manually, then using these values as the initial inputs to the fitting algorithm. In some cases, the

function tolerance needed to be relaxed to prevent the algorithm from iterating past a reasonable solution.

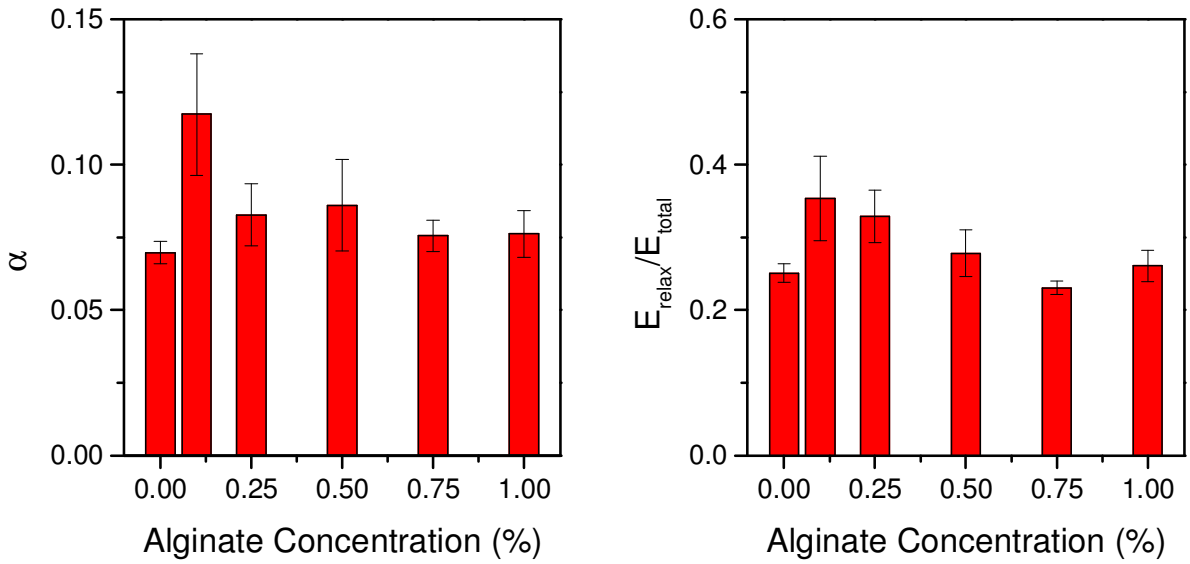

Figure 8. (a) Average value of **α** using the KVFD model and (b) average ratio of relaxation moduli to the total calculated modulus using the GM-5 model. Uncertainty bars represent the standard error in the sample mean. For these results, 5-8 samples were tested at each alginate concentration.

In an effort to determine whether the toughness increase in gelatin/alginate samples was reflected in a corresponding change in the viscoelastic model parameters, the fit values of α (for the fractional models) as a function of alginate concentration was examined, as this parameter is tied to the degree of viscous relaxation occurring within these samples. As seen in Figure 8a, there was no statistical difference between the values of α for the different alginate concentrations ($p = 0.174$). The value of α does spike at low alginate concentrations, but this is believed to be due to outliers in the data. A similar metric can be calculated for the GM-5 model fits by calculating the ratio of the sum of the coefficients in front of the exponential terms to the total modulus, which can be calculated by adding up all the "E" terms. This plot is shown in Figure 8b, and once again, there appears to be no statistical difference across the different alginate concentrations ($p = 0.112$).

In fact, no statistically relevant trends were found between any of the modeling parameters across the different alginate concentrations tested. These results suggest that at low strains (up to ~5%) and strain rates (~0.5% s^{-1}) utilized in these initial ramp-hold tests that the addition of sodium alginate, while enhancing the toughness of the samples, does not appreciably affect the mechanical properties of the gelatin, which could be of interest for designing test phantoms for particular applications.

In order to further explore the observed toughness enhancement observed in the gelatin/alginate samples, additional stress relaxation experiments were run at a much higher ultimate strain (25%). As noted in the Methods section, at larger strain the gelatin samples deviate from linear elastic behavior, precluding modeling the entire ramp-hold strain profile. Instead, a faster strain rate in the ramp region was used to provide an abrupt increase in strain to ε_{max} = 25%, and the relaxation in these samples was modeled with a five-term Prony series, which is the analytical solution to the GM-5 model for a step change in strain.

$$E(t) = \frac{\sigma(t)}{\epsilon_{max}} = E_0 + E_1 \cdot \exp\left(-\frac{t}{\tau_1}\right) + E_2 \cdot \exp\left(-\frac{t}{\tau_2}\right) \tag{14}$$

By utilizing the GM-5 model for modeling the stress relaxation (or equivalently, modulus relaxation) for these high strain samples, the relative contribution of shorter-term and longer-term relaxation effects can be observed by restricting the fitting parameters to include only two time constants: τ_1 (on the order of 3 – 5 s), which represents the short-term relaxation effects, and τ_2 (on the order of 90 – 150 s), which represents longer-term relaxation effects.

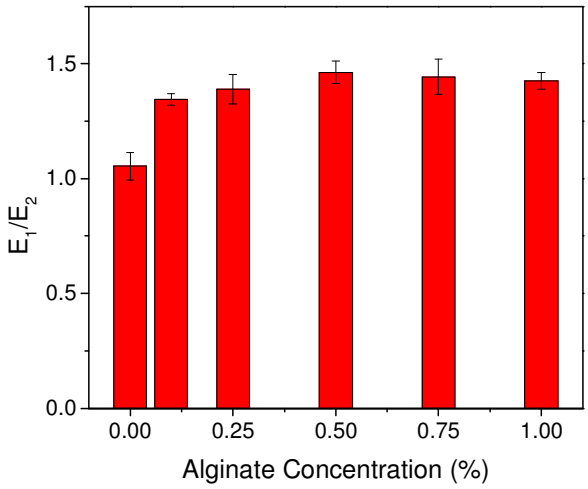

Figure 9. Average value of E_1/E_2 for high strain force relaxation experiments. Uncertainty bars represent the standard error in the sample mean. For these results, 6-8 samples were tested at each alginate concentration.

Figure 9 shows how the metric E_1/E_2, which represents the ratio of the magnitude of short-term relaxation versus the magnitude of long-term relaxation, varies as a function of alginate concentration. As the concentration of alginate in the sample increases, E_1/E_2 increases. Also, the value of E_1/E_2 for neat samples was smaller than for all alginate-containing samples. This indicates that adding alginate to gelatin results in a shift in stress relaxation to shorter time scales. This trend could help to explain the observed toughness enhancement when adding alginate to gelatin samples. Mechanistically, if a sample has the ability to relax more quickly, it can more easily dissipate energy, which would result in an increase in the sample's toughness. Furthermore, the observed trend is very similar to the trend observed in the strain-to-break of these samples (Figure 9c), which further supports this hypothesis.

Others have shown previously that, for pure gelatin systems, short-term relaxation can be associated with fast moving fluid flows within the hydrogel matrix, and longer-term relaxation can be associated with the restructuring of the matrix itself.[26] An increase in the short-term relaxation modulus therefore suggests that sodium alginate increases the viscous character of the hydrogel at high strains. In regards to the observed toughness increase, the enhanced viscous

character of the sample would presumably also be responsible for energy dissipation at high strains, which would offset chain relaxation and broken crosslinks, and lead to a high strain-to-break.

3.3 Analysis of structured water content with TGA

If the improved mechanical properties can be tied to changes in the fluid portion of the hydrogel matrix, as the ramp-hold relaxation data would suggest, then the next step would be to probe this region. One common way to probe the fluid region of the hydrogel matrix is to perform thermal experiments such as TGA or differential scanning calorimetry (DSC).[15, 44] Water within the hydrogel matrix exists in three main states: non-freezable bound water, freezable bound water, and bulk water.[45] Non-freezable bound water refers to water bound so tightly to the polymer matrix that it is unable to interact with neighboring water molecules and crystallize, even at temperatures as low as -100^{o}C.[45] Freezable bound water refers to structured water which interacts with the polymer matrix, but is still able to crystallize when the temperature is lowered below 0^{o}C. This state of water will have a freezing point below that of pure, unbound water.[45] The final state of water is bulk water, which interacts weakly or not at all with the polymer matrix, and freezes around 0^{o}C.[45] Presumably, these states of water could also be measured by observing the liquid-vapor phase transition with TGA rather than the liquid-solid phase transition with DSC, although the comparison is not perfect since bulk water can evaporate well below the boiling point and no specific orientation of water molecules is required for the liquid-vapor phase transition. However, it would still be expected that bulk water would evaporate at a lower temperature than water bound to the polymer matrix.

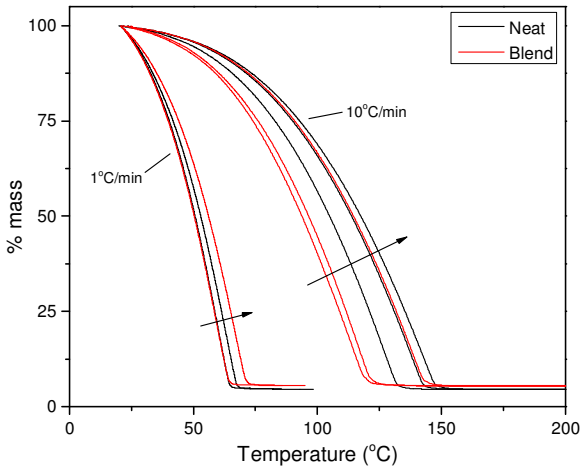

Figure 10. Thermogravimetric curves for neat (black) and blend (red) samples at heating rates of 1°C min^{-1} and 10°C min^{-1}. Arrows represent an increasing initial mass of the samples.

Figure 10 shows the thermogravimetric curves for fully-hydrated gelatin (5% w/w) and gelatin/alginate blend (5/1% w/w) samples. A thermogravimetric curve displays the percent of the initial mass remaining as a function of temperature. Initially, all mass lost is due to the evaporation of water, but at higher temperatures the decomposition of gelatin and alginate can be observed (not pictured).

When the samples are heated at a rate of 10°C min^{-1}, the percent mass remaining following water loss levels off to approximately 5.3% for alginate-containing samples and 4.4% for pure gelatin samples. These values are not dependent on either the initial mass of the sample or the heating rate. These values are slightly off from the predicted values of 6% and 5% for the blend and neat samples, respectively. Based on their thermogravimetric curves, the dry gelatin and sodium alginate powders were found to contain approximately 12% w/w and 15% w/w of water, respectively, and including this water completely accounts for the difference between the observed and expected sample mass at the end of the water loss period. Regardless, the difference between the two is nearly the expected value of 1%.

These thermogravimetric curves can also be used to look at the rate of evaporation from these samples. Presumably, if water within the matrix was bound more strongly to the polymer matrix, it would take more energy to remove it, which would result in a higher temperature at which all water was finally evaporated (the point where the curve levels off). However, interactions with the polymer matrix are not the only explanation for differences in this level-off temperature. In order for water to evaporate from the sample, it has to move from the interior of the sample to the surface before it can escape. This means that in addition to changes in the interaction between water and polymer, there may also be diffusion limitations or transport effects which could vary based on the initial size of the sample. This problem is made even more complicated by gelatin's melting point at around 23-30°C.[4] At the beginning of the period of water loss, the samples are roughly cubic, but as the temperature increases the sample melts to form a pool, which can take different amounts of energy based on the initial size of the sample. To limit these effects as much as possible, a second set of trials were performed at a lower heating rate (1°C min^{-1}) to hopefully maintain thermal equilibrium throughout the test (Figure 10).

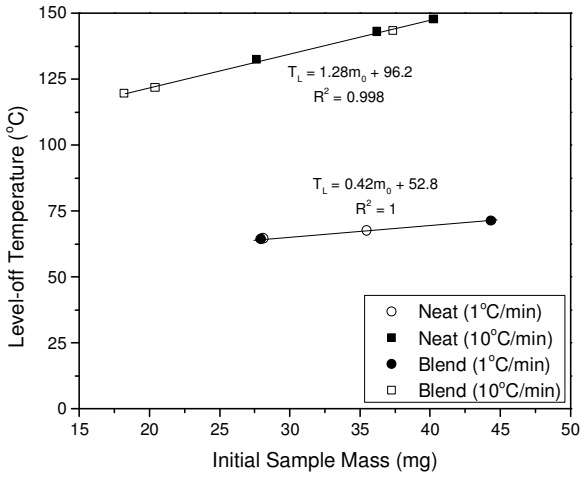

Figure 11. Level-off temperatures as a function of initial sample mass for both neat (5% w/w) and blended (5/1% w/w) samples at both high (10°C min^{-1}) and low (1°C min^{-1}) heating rates.

Figure 11 shows the level-off temperature as a function of the initial sample mass for both the neat and blended samples at both the high and low heating rates. Based on this data, it appears that over the range of initial sample masses and heating rates tested the level-off temperatures are linearly related to the initial sample mass for a given heating rate and are not dependent on whether the sample contains alginate. Based on the results from TGA, the presence of alginate seems to have little to no effect on the amount of bound water within these hydrogels. This could be a result of the total amount of water present in these samples. Djabourov et al. estimated from ^{1}H-NMR that gelatin contains around 0.45 grams of bound water per gram gelatin.[2] From this result, it is expected that only 2.4% of the water present in a 5% w/w gelatin sample would be bound to the polymer matrix and slightly more for the gelatin/alginate blend. Since the expected difference in structured water content is so minor, it is possible this technique lacks the sensitivity to identify any dissimilarities in these fully-hydrated samples.

3.4 Effect of pH on mechanical properties

With thermal analysis suggesting that differences in structured water within the hydrogel matrix are not behind the observed toughness enhancement, new mechanisms must be considered. The next logical consideration is that the polymers themselves are interacting rather than the water. Interactions between gelatin and sodium alginate could take the form of hydrogen bonds, electrostatic interactions between charged groups, or dispersion forces, however, a recent publication found that the attractive interactions between sodium alginate and fish gelatin were mainly electrostatic.[30] The simplest way to change the charge of a polymer is to change the pH of the solution, so a series of mechanical tests were carried out on neat and blend samples while varying the pH of the samples. The pH was adjusted with 1.0 N NaOH or HCl and no buffer was

used. The pH adjustment will also change the ionic strength of the solution, but this effect was not accounted for.

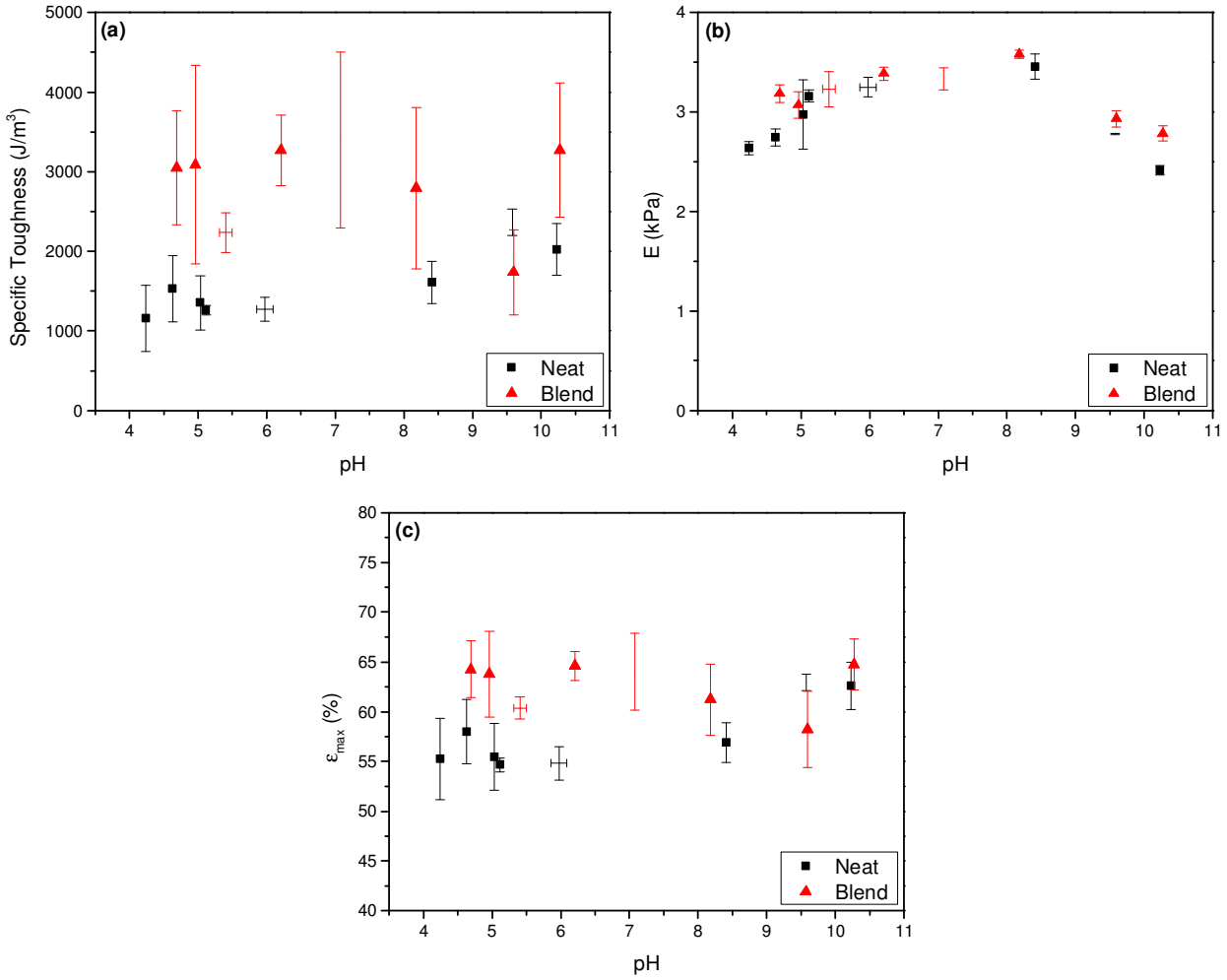

Figure 12. (a) Specific toughness, (b) elastic modulus, and (c) strain-to-break as a function of pH for neat (5% w/w) and blend (5/1% w/w) samples. Uncertainty bars represent one standard deviation. Where uncertainty bars are shown, but no point, only two points were available.

Figure 12 shows the mechanical properties of neat (5% w/w) and blend (5/1% w/w) samples as a function of pH. All data were taken using the second batch of gelatin mentioned earlier. The pK_a values of the amino acids discussed in the following sections are for the free amino acids in solution and are expected to shift slightly in the protein chain. The Young's moduli of neat and blend samples (Figure 12b) are within statistical uncertainty over the neutral pH range from about 5 to 9 with both formulations reaching their maximum stiffness at around

pH 8.5. In this range, the carboxylate groups on both uronic acid residues in sodium alginate are expected to be completely deprotonated and the only relevant amino acid with a pK_a in this range is histidine at 5.97.[6] Since gelatin contains very little histidine (< 1%), it is unlikely there is any significant change in electrostatic interactions over this pH range.[3, 5]

There is a noticeable drop in Young's modulus at pH < 5, most likely due to the protonation of glutamic acid (pK_a = 4.25) and aspartic acid (pK_a = 3.65) side chains. This results in gelatin chains with a more positive overall charge, resulting in greater electrostatic repulsion between neighboring chains and preventing the formation of junction zones. A similar effect is observed at pH > 9, most likely due to the deprotonation of lysine (pK_a = 10.28) and, to a lesser extent, arginine (pK_a = 13.2) side chains. The resulting gelatin chains carry a more negative overall charge and, again, increased electrostatic repulsion between neighboring chains will result in fewer interchain interactions and weaker gels. At even larger pH values, it appears that blend samples experience a smaller drop in modulus than neat samples although additional trials are needed to confirm this trend.

Comparing Figure 6a and Figure 12a, a similar observation can be made regarding the toughness and strain-to-break of blended samples. Samples containing sodium alginate have a larger toughness over the entire pH range, excepting a single point around pH 9.5. Additional trials should be run at this pH to determine whether this point is truly an anomaly. Ignoring this point, there is no clear relationship between pH and toughness for either the neat or blend samples.

One rather noticeable feature of Figure 12a is the large variance, especially in the blended samples. While the data is good enough to make quantitative comparisons of the average

toughness of neat and blended samples over the entire pH range, there is far too much uncertainty to determine if the toughness of alginate-containing samples varies with pH.

Several possible sources of error which stem from the sample preparation and testing method can be explained. For example, since gelation is both a kinetic and thermodynamic process, the temperature at which the samples are stored can have a large effect on the triple helix content of the cured gels, which in turn affects the elastic modulus.[2, 8, 46] Others have also reported as much as a 20% decrease in the elastic modulus when the storage temperature is increased from 21.5°C to 24°C, and stressed the importance of maintaining < 1°C differences in the storage temperature between batches to minimize systematic error.[28] During these experiments, no such temperature control was implemented.

3.5 Qualitative comparison of unconfined, parallel plate compression-to-failure and confined, spherical indentation puncture tests

The previous set of experiments was repeated using a confined puncture test with a spherical indenter with the hope of confirming the results of the previous test and reducing the uncertainty in the data so that conclusions could be drawn regarding the underlying mechanism. In order to validate this new testing procedure, an adhesion test was first run to determine if adhesive forces could be considered negligible, allowing for the use of Hertzian contact theory, or not, which would require a more complicated theory such as the Johnson-Kendall-Roberts model. To minimize adhesive forces, the space above the sample was filled with water and the indenter submerged. A three-cycle adhesion test (Figure 13) was then performed on both a lubricated and unlubricated sample by compressing each sample to a maximum depth of ~1.5 mm (2% strain) before decompressing the sample past the initial point of contact.

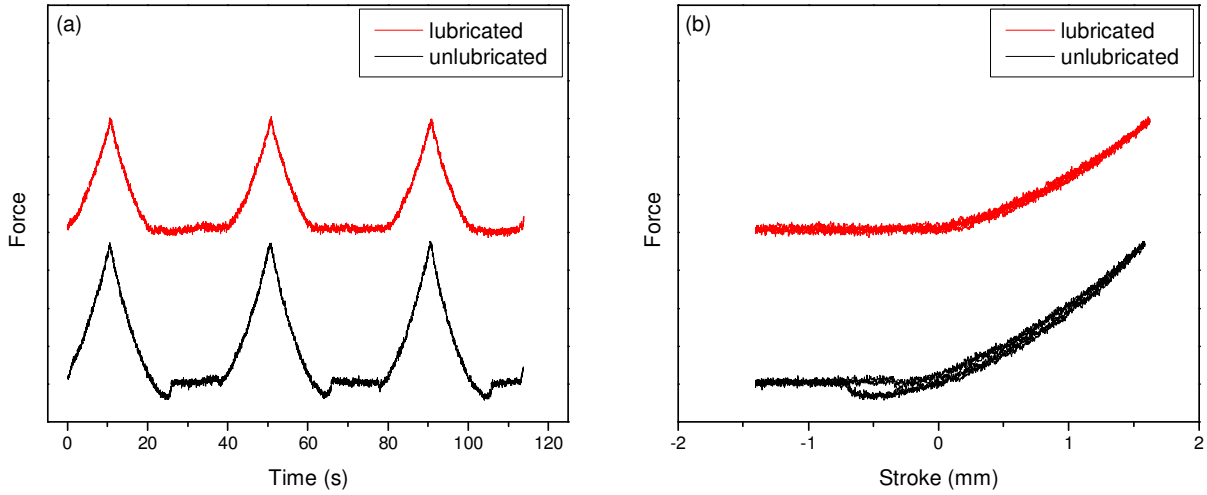

Figure 13. Adhesion test performed on both an unlubricated and lubricated sample using a spherical indenter. (a) Force response over three complete cycles as function of time and (b) hysteresis of the force response over the same three cycles.

A negative force when raising the indenter past the initial point of contact would indicate the presence of significant adhesive forces. The unlubricated sample in Figure 13a clearly shows the indenter sticking during the unloading portion of the test. The lubricated test, on the other hand, shows no such sticking force. Figure 13b shows the same data set as a function of indenter position. Clearly, the unlubricated sample showed the same sticking force, but for the lubricated sample there was minimal hysteresis over three cycles. The adhesion test of Figure 13 was performed at very low compressions (< 0.05 N) and may not be perfectly applicable over the entire range of forces that occur during the puncture test.

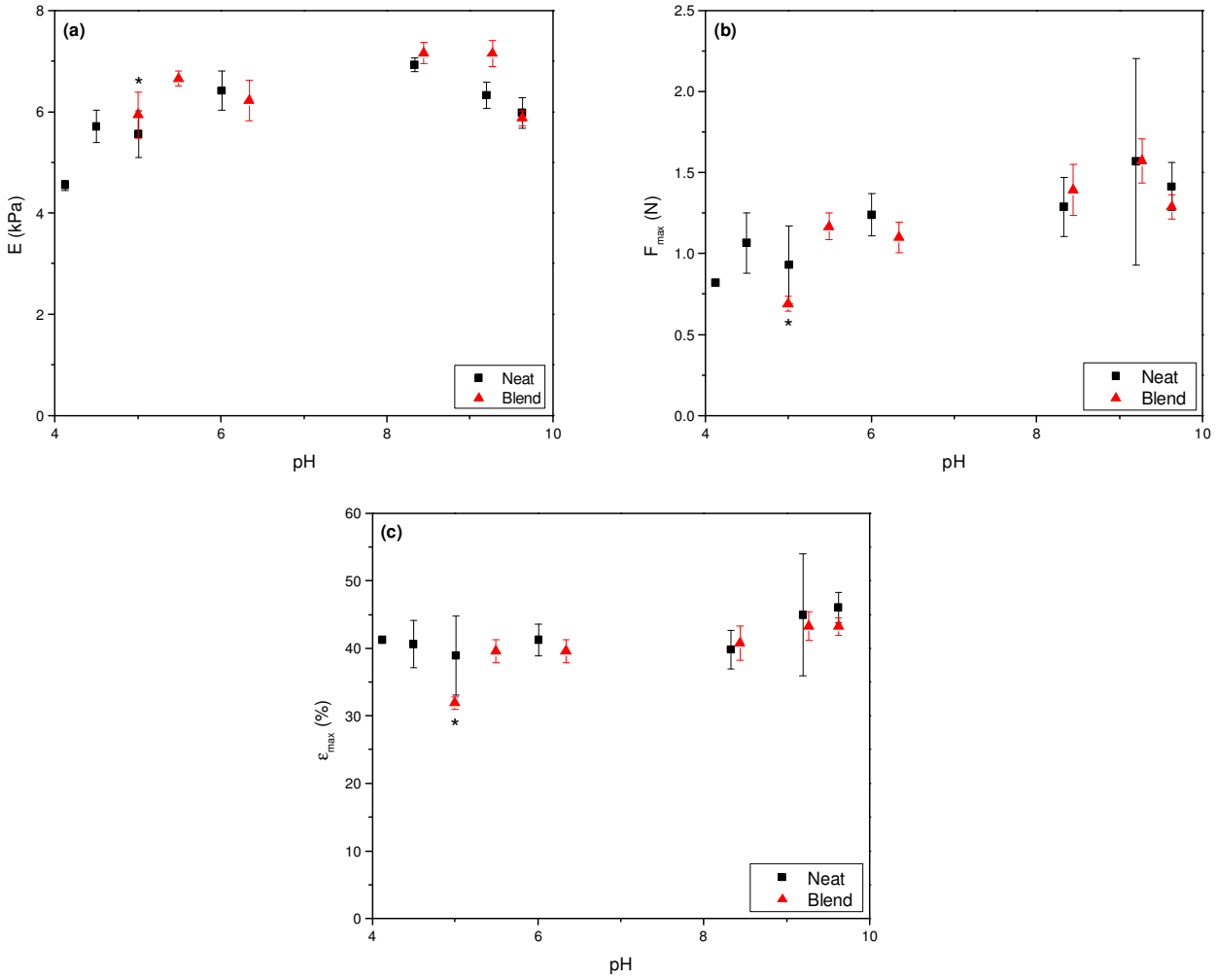

Figure 14. (a) Young's modulus, (b) puncture force, and (c) strain-to-break for 5% w/w neat gelatin and 5/1% w/w gelatin/alginate samples using spherical indenter. Uncertainty bars represent one standard deviation. The blend sample indicated by a star (*) was opaque, unlike every other sample tested, most likely a result of phase separation.

The mechanical properties of both sets of samples as a function of pH as determined by the puncture test can be found in Figure 14. As a reminder, there were two main reasons for performing a puncture test. First, by using a second type of failure test, it could be determined whether the previously observed toughness enhancement was real or an artifact of the parallel plate testing procedure. Second, the data from the parallel plate compression-to-failure experiments (Figure 12) were highly uncertain. Although qualitative comparisons of the two

sample types could be made, this uncertainty was too large to determine whether the toughness determined by the parallel plate experiment was affected by pH and no conclusions could be drawn regarding the underlying mechanism. This noise was believed to be attributed to a lack of lubrication at the sample-testing head boundary, the absence of a clear point of failure in many experiments, and surface defects in the samples as a result of the de-molding process, all of which could be corrected by this new procedure.

The results in Figure 14a show that the elastic moduli of neat and blend samples over the entire pH range tested are within statistical uncertainty. These values are roughly constant between pH 5 and 9, reaching a maximum value at around pH 8.5. This is the same trend that was observed in the unconfined, parallel plate experiments (Figure 12b) and both are in good agreement with previous reports for gelatin.[47] Unlike the results of the parallel plate test, however, there was no discernible difference in moduli at the extremes of the pH range. Additional experiments will need to be performed to determine whether the trend exists or was a statistical anomaly. The Young's modulus calculated from the puncture test is roughly double the measured value from the parallel plate experiment. The reason for this increase will be discussed in detail later.

The puncture force as a function of pH can be found in Figure 14b. The data shows an extreme contrast with previous results (Figures 6a and 12a). The toughness enhancing effect has disappeared completely. It is possible the puncture test is not a perfect surrogate for the parallel plate test and does not adequately measure a sample's bulk toughness or there may be a separate effect that causes blend samples to perform better during the parallel plate test. Some possibilities will be discussed later. As before, the strain-to-break (Figure 14c) tracks almost

perfectly with the puncture force, which makes sense given the nearly constant modulus over most of the pH range.

It needs to be mentioned that the puncture tests were carried out using a different batch of gelatin than previous experiments. Most notably, the native pH of a 5% w/w gelatin solution dropped from 6 to 4.5. At this pH, the gelatin chains are positively charged and can form complexes with alginate polyanions. When alginate was added with no pH adjustment, the pH increased to 5 and the cured gels were opaque (Figure 15), indicating the formation of insoluble gelatin-alginate complexes leading to liquid-liquid phase separation (complex coacervation) or gelatin-alginate precipitates. Razzak et al. recently observed the same phase separation in dilute fish gelatin-alginate systems and were able to create a phase diagram for the formation of gelatin-alginate complexes as a function of pH and the protein-to-polysaccharide ratio.[30] Based on their results, it is believed the phase separation reported here is due to complex coacervation between the two macromolecules, although some precipitation may have occurred. This phase separation made it impossible to create samples at pH values less than 5. Unconfined parallel plate experiments were not performed on this gelatin batch.

Figure 15. Phase separation in blend samples at pH 5 using the third gelatin batch.

As mentioned previously, the elastic moduli calculated during the puncture test were roughly double the values measured during the parallel plate experiments. The Young's modulus for the puncture test can be calculated from Hertzian contact mechanics as follows. The force applied between an elastic, spherical indenter and an elastic semi-infinite plane is given by the equation:

$$F = \frac{4}{3} E^* R^{1/2} d^{3/2} \tag{15}$$

where F is the applied force, R is the radius of the indenter, d is the depth of the indentation and E^* is a weighted average of the Young's moduli of the two materials given by:

$$\frac{1}{E^*} = \frac{1 - \nu_i^2}{E_i} + \frac{1 - \nu_s^2}{E_s} \tag{16}$$

where E_i and E_s are the Young's moduli of the indenter and sample, respectively, and ν_i and ν_s are the Poisson's ratio of the indenter and sample, respectively. Since the indenter is made of aluminum, which is several orders of magnitude stiffer than these samples, the first term on the right side of Equation 16 can be eliminated. The Poisson's ratio of gelatin hydrogels of roughly the concentration used here have been shown previously to be between 0.47 and 0.5.[26] Assuming this value to be 0.5, the Young's modulus of the sample can be solved for as:

$$E_s = \frac{9F}{16R^{1/2}d^{3/2}} \tag{17}$$

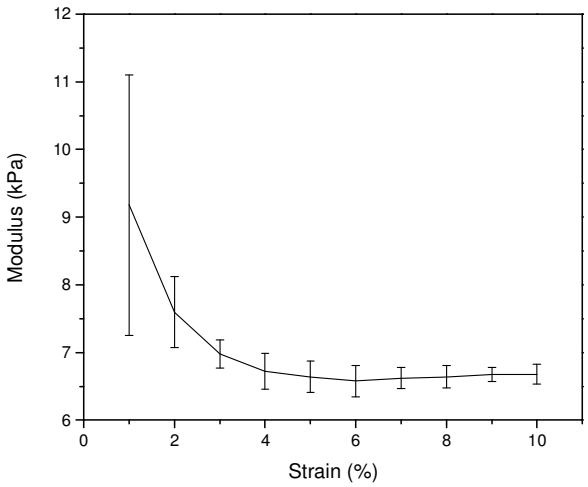

Figure 16. Young's modulus as a function of strain during puncture tests performed on four 5/1% w/w blend samples at pH 5.49. Each point is the average modulus of the four samples and uncertainty bars represent one standard deviation.

Figure 16 shows the Young's modulus as a function of strain for a set of puncture tests performed on four 5/1% w/w blend samples. The curve was generated by using experimental data to calculate the Young's modulus with Equation 17. At low strains (1-2%), the calculated modulus is approximately 9 kPa, dropping to around 6.6 kPa at strains up to 10%. These values are clearly larger than values measured by parallel plate compression tests, which means only qualitative comparisons can be made between samples tested using different methods. Best practice dictates that the elastic modulus is measured at as low a strain as practically possible to ensure the material is still within the linear elastic region. Based on Figure 16, however, it is clear this method is not appropriate when compressing these confined samples with a spherical indenter. Instead, the modulus was calculated by fitting experimental data with Equation 15 and minimizing the sum of squared errors between 6 and 10% of the sample height. This range was chosen because the modulus vs. strain curve was level in this region across all samples (Figure 16).

The value the curve in Figure 16 levels off to is still significantly larger than any of the values measured during parallel plate tests. This over-estimation of the Young's modulus is most

likely due to the confined samples being too small relative to the size of the indenter, causing the walls of the mold to affect the force measurement. The two primary metrics for these sample dimensions are the ratio of the sample and indenter diameters and the ratio of the sample height to the indenter diameter.[48] The general rule of thumb for spherical indentation is for the sample diameter to be at least 10 times the diameter of the indenter.[35] In the test reported here, this ratio is ~4.4, which means the walls of the mold may affect the force measurement. Others have previously performed a similar test on gelatin samples, and found that at this concentration and approximate dimensions, there was a significant over-estimation of the modulus.[48]

As mentioned previously, the Young's modulus is most accurately measured at very low strains; however, the other striking feature of Figure 16 is the large uncertainty in the modulus at low strains. Others have observed this same effect in the relaxation modulus of gelatin hydrogels.[49] They observed this large uncertainty for indentation depths up to 15% of the indenter radius, which for this experiment corresponds to a strain of approximately 2%. The authors attributed this large uncertainty to difficulty in determining the initial point of contact and instrument noise due to the extremely low measured force at these indentation depths.[49]

All of these observations were repeatable and Figure 17 shows a plot of the elastic modulus as a function of strain for both samples across the entire pH range.

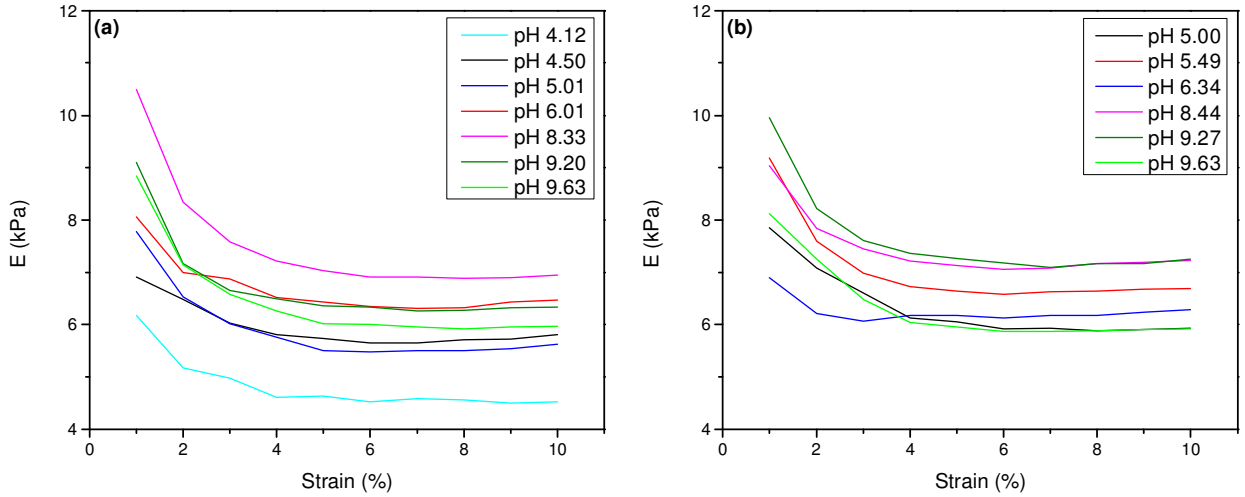

Figure 17. Young's modulus as a function of strain for (a) neat and (b) blend samples.

Returning to the disappearance of the toughness enhancing effect, Figure 18 shows an example force-displacement curve for a puncture test. The force-displacement curve for the neat gelatin sample shows a drop in force at a displacement of about 7 mm with continued perturbations in the force up until the point of failure. These deviations could have a number of causes including sudden delamination of the sample from the mold, adhesion between the sample and indenter tip at larger forces, or minor fractures in the sample not significant enough to cause failure. Since, visually, no delamination or partial fracturing was observed, the most likely cause for this drop in force is believed to be a lack of lubrication between the sample surface and indenter tip causing the surface to slip.

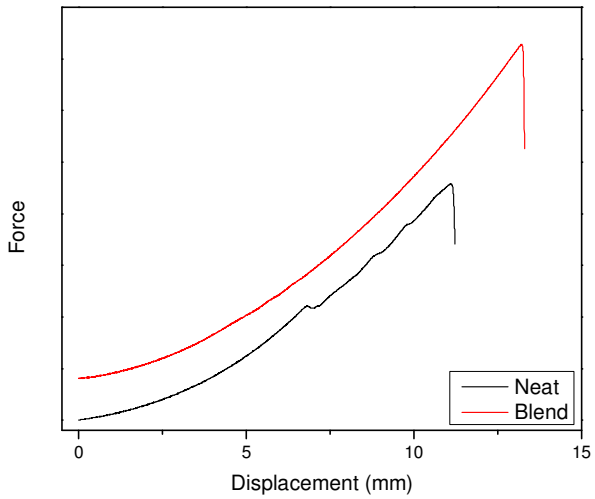

Figure 18. Sample force-displacement curves from spherical puncture tests. The black line is a neat gelatin sample prepared at pH 8.33 and the red line is a blend sample prepared at pH 8.44. The force-displacement curve for the blend sample has been shifted up 0.2 N for visualization purposes.

One interesting feature of Figure 18 is that only the neat gelatin sample shows this perturbation. In fact, this occurred in 19 of the 28 neat gelatin samples tested. By contrast, not a single blend sample exhibited this behavior. From this result, there is a strong possibility there is some difference between neat and blend samples at the surface. Having several groups which can participate in hydrogen bonding, sodium alginate, like gelatin, is a very hydrophilic macromolecule. Alginate molecules at the surface of blend samples may more strongly attract the water being used as a lubricant, creating a thicker layer of bound water at the interface and increasing lubrication between the indenter tip and the surface.

If alginate does increase lubrication at this interface, it could explain the disparity between the results of the parallel plate, compression-to-failure and puncture tests. In the parallel plate tests, when the sample ultimately failed, the initial crack nearly always propagated where the edge of the sample was in contact with either the top or bottom plate. Any adhesion between the sample and the plate would result in a radially inward traction. Since the samples are roughly incompressible, as they are deformed, a Poisson effect will cause them to expand radially

outward. Combined, these two forces create the observed bulging behavior (Figure 5f). As a result, a localized increase in stress would be created within the material that may cause premature failure.

In an idealized toughness test, the absorbed energy should be distributed evenly throughout the sample as much as possible. Clearly, in the parallel plate, compression-to-failure tests reported here, this was not the case. It may be that this test did not adequately measure the bulk toughness, and instead measured the force required to tear the sample at the preceding edge, which would be a function of the actual toughness as well as any adhesive forces. Furthermore, any imperfections at this edge such as those in Figure 5a-c and discussed earlier would cause the sample to fail even more prematurely. Therefore, if the alginate-containing samples do indeed have a lower adhesion force between surface and indenter, there would be less stress focused at the preceding edge, resulting in a larger observed toughness measurement.

Since lubrication effects seem to be the cause of the perceived toughness increase, one way to confirm the result of the puncture test would be to run a tensile failure test, rather than the compression one that was used. In a tensile test, the samples would still be prone to crack propagation from any surface defects, but any differences in adhesion could be eliminated. Also, coating the indenter with Teflon spray or using a non-polar lubricant such as mineral oil may yield a different result.

3.6 Contact angle measurements

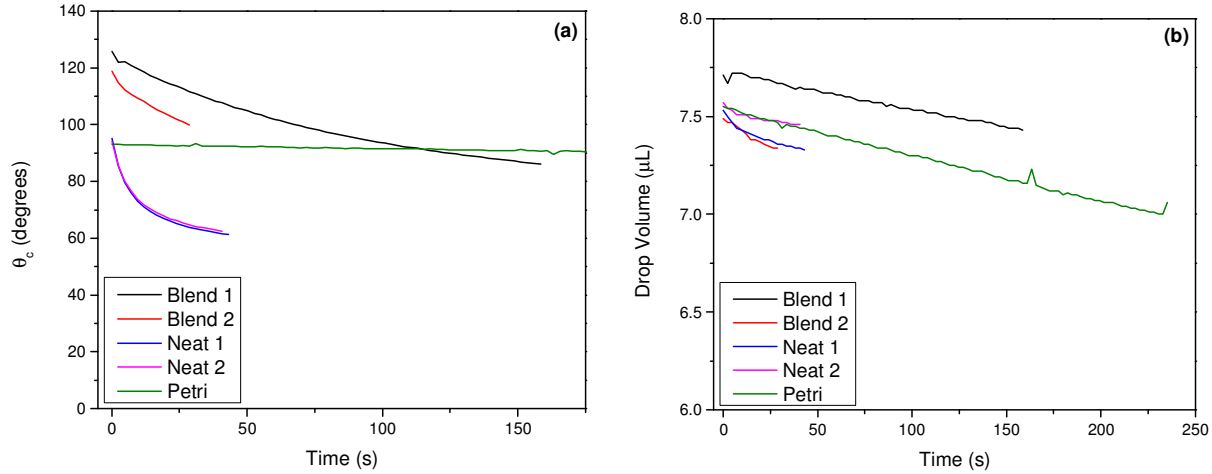

Figure 19. Contact angle as function of time for a fully-hydrated neat sample (pH 6.04), a fully-hydrated blend sample (pH 5.97), and a polystyrene surface. Two trials were run on each hydrogel sample.

Based on the results of the confined puncture test, it was believed there was a measurable difference between the surfaces of the neat and blend samples which resulted in improved lubrication in the latter which may be due to a change in the hydrophilicity of the surfaces. The way the hydrophilic character of a surface is most commonly measured is by placing a sessile water droplet on the clean surface and measuring the contact angle with a goniometer.

Figure 19a shows the contact angle of a sessile water droplet on the fully-hydrated surface as a function of time for both a neat and blend sample at pH 6. The initial contact angle for the neat sample was around 95^{o} and 123^{o} for the blend samples. Both gelatin and alginate are water-soluble biopolymers, so it is interesting that a blend of these could produce a hybrid material which is hydrophobic. This unusually high contact angle for gelatin hydrogels has been observed by other researchers, with contact angles ranging from 90^{o} all the way up to 124^{o}.[50] In Figure 19a, the initial contact angle for the neat sample is around 95^{o} which is on the low end of this range; however, the contact angle in hydrogels is a function of polymer concentration and the gel hydration state. Although likely not a complete explanation, the underlying mechanism

behind the large contact angle for many hydrogels is the preferential movement of hydrophobic moieties to the hydrogel-air interface.[50, 51] These hydrophobic groups are repelled by the water in the bulk phase and, therefore, it is energetically favorable to move to the hydrogel-air interface where fewer water molecules are present.

One factor which controls a hydrogel's potential to attract water is the extent to which the polymer is ionized. As the number of available charges decreases, so does the ability of gelatin chains to attract water. For example, one characteristic of the isoelectric point is that the net charge of the protein is at a minimum and fewer charged groups are available to attract water.[52] At this point gelatin experiences a minimum in swelling in an aqueous medium.[53] It is possible the increase in hydrophobicity could be caused by the formation of charge-neutral, soluble gelatin-alginate complexes which would produce a material with fewer overall charges available to attract water.

Since these hydrogels are comprised of mobile polymer chains, the surface is able to restructure itself over time to minimize the surface energy. A comparison between both hydrogel samples and a polystyrene Petri dish in Figure 19a shows that this restructuring can result in significant changes in the contact angle. As more hydrophilic groups migrate to the surface, the result is a decrease in contact angle which is observed in Figure 19a. Based on the contact angle versus time profiles, it appears the contact angle of the neat sample decreases more quickly on shorter time scales. This would suggest the blend samples have less chain mobility as it takes longer for hydrophilic groups to migrate to the surface. This could be due to the gelatin-alginate complexes mentioned earlier acting as crosslinks or to chain entanglements at the higher solids concentration. It is likely the contact angle would level off to some equilibrium value; however, these experiments were not run long enough to predict this value with any degree of confidence.

The 25% strain stress relaxation data fit earlier with a five-parameter Prony series found the addition of 1% w/w sodium alginate decreased the long-term relaxation time constant from approximately 140 s to 110 s, which is the opposite effect of what was observed by contact angle measurements.

Since the blend samples are more hydrophobic, they form a higher energy interface when submerged in water. In order for the material to failure, a crack must first form, which will result in an increased surface area. Since the blend samples have larger interfacial energies when underwater, more energy is required to create this new surface, which would result in an increased tearing energy and cause them to appear tougher. Several new experiments would need to be performed to determine if more energy is indeed required to tear the surface of a submerged blend sample.

Figure 19b displays the volume of the water droplet as a function of time for the same trials as Figure 19a. Since the testing apparatus is open to air and not in a humidified chamber, the water droplet will evaporate over time. Water could also be lost through absorption into the hydrogel. If there is any pinning at the edge of the droplet, water loss occurring by either mechanism could lead to a changing contact angle even in the absence of any surface restructuring. Comparing the rate of water loss for each of the hydrogel trials to a control using a nonporous polystyrene surface suggests that neither sample absorbs an appreciable amount of water.

4. CONCLUSIONS

Gelatin as a biomaterial suffers from poor mechanical properties and generally requires some type of crosslinking to be viable in many applications. Although gelatin is an ideal material

for tissue phantoms, its brittleness makes it a difficult material to work with as handling it is often enough to damage the delicate surface. Initially, it was found that adding up to 1% w/w of sodium alginate to gelatin hydrogels could increase the toughness of these materials by as much as 150% without significant changes in the Young's modulus, the most important parameter for mimicking biological tissue. The result would be a tissue phantom with biologically accurate stiffness which could hold up to mechanical handling while maintaining a pristine surface.

Quasi-static stress relaxation experiments were performed to characterize the linear viscoelastic properties of these materials. The resulting stress-time profiles were fit with three different linear viscoelastic models: the Generalized Maxwell model, the Kelvin-Voigt Fractional Derivative model, and the Maxwell Fractional Derivative model. It was found that the two fractional calculus-based models, which more closely resemble a power-law fit rather than an exponential, produced more accurate fits of the experimental data in terms of the resulting sum of squared error. At larger strains, the fractional calculus models could no longer be used and, using the Generalized Maxwell model, it was found that the alginate-containing samples experienced a shift in overall stress relaxation to shorter time scales, which has been shown previously to be associated with fluid flows within the hydrogel matrix.

In order to probe the fluid region of these hydrogels TGA was carried out in order to analyze the liquid-vapor phase transition. Although structured water makes up only a small portion of the total water in these highly hydrated materials, the hope was that if differences were found they could be tied to an increase in viscous dissipation, which would lead to the observed toughness enhancement. The amount of bulk water in these samples obscured any dissimilarity between the two sample types and, further, it was found that the liquid-vapor transition was largely dominated by transport effects.

In many viscoelastic materials, the behavior occurs as a result of electrostatic interactions between ionic and/or polar groups breaking and reforming repeatedly to dissipate energy. In order to study how electrostatic effects contribute to the overall mechanical properties, another series of parallel plate compression-to-failure tests were carried out while varying the pH at which the hydrogels were prepared. It was found that the Young's moduli of these materials were indiscernible at neutral pH although the alginate-containing samples may be stiffer under highly acidic or basic conditions. This effect was not observed during puncture tests. The parallel plate test also confirmed the previously observed toughening effect, although the data was too noisy to determine if toughness was a function of pH in either material. This noise was largely attributed to inadequate lubrication at the interfaces with both testing plates, the lack of a clear break point, and to a number of surface defects which occurred during the de-molding procedure.

In order to eliminate these sources of error, a confined puncture test with a spherical indenter was performed, believing that the same toughness enhancing mechanism would lead to a larger puncture force in the alginate-containing samples. Since the samples did not have to be de-molded, the errors associated with surface defects could be eliminated. These tests also had very clear endpoints. The Young's moduli calculated from this experiment qualitatively matched the previous results and the quantitative differences were likely associated with the confined nature of the test. While the confined puncture test did indeed produce more consistent data, the toughness enhancing effect of alginate which was the basis of this report, was no longer observed.

During the confined puncture tests, several samples experienced a sudden drop in force which was attributed to adhesion between the surface and indenter tip. Interestingly, while the majority of neat gelatin samples exhibited this behavior, not a single alginate-containing sample

did. This could be due to enhanced lubrication at the sample/water interface. The increase in lubrication could also be used to explain the observed toughness increase in the parallel plate experiments. It was visually observed during these experiments that initial failure occurred at the outer surface of the sample, often at the sample/plate interface and it may be possible that every sample failed prematurely. It is believed that alginate, at the concentrations used, may have no effect on the bulk mechanical properties of gelatin hydrogels and the perceived toughness increase during parallel plate compression-to-failure experiments was governed not by the bulk properties of the material, but by the adhesive forces between the sample and the plates.

5. FUTURE WORK

Based on the results of the various mechanical tests performed, there is reason to believe the addition of sodium alginate to gelatin hydrogels can alter the surface properties of these materials even in relatively small concentrations. Based on preliminary sessile drop contact angle measurements, the surfaces of the gelatin/alginate blend gels are much more hydrophobic than gelatin alone. When tracking the contact angle as a function of time, the surfaces of both the neat and blend samples became more hydrophilic indicating either the ability of the surface to restructure itself or the diffusion of ions present in the hydrogel into the water droplet, decreasing the surface tension of the droplet. The initial rate of this transition was greater in neat samples, possibly due to decreased chain mobility in blend samples due to electrostatic interactions between gelatin and alginate or mechanical entanglement between chains.

The contact angle results reported here were taken on only a single surface of each type. Additional trials are necessary to confirm both whether the blend samples are more hydrophobic than their neat counterparts and if the surface of the blend samples restructures more slowly.

Also, the trials that were performed were on relatively small time scales. It may be useful to perform longer experiments (perhaps on the order of ~30 minutes) to look at both the short and long-term restructuring behavior of these surfaces and determine if an equilibrium contact angle can be reached in a reasonable time. Additionally, these measurements could be taken while varying the pH and ionic strength of the samples. These results could then be modeled and provide insight into how the ultimate mechanical properties of the materials were affected in the unconfined, parallel plate compression-to-failure experiment.

Since the contact angle experiments seem to suggest the importance of understanding the surface behavior of these materials in addition to the bulk properties, analyzing the morphological characteristics of the surface with scanning electron microscopy (SEM) may provide some useful insights. SEM could be used to compare the surface and bulk morphologies of these samples. Another interesting experiment would be to cover the surface of a freshly prepared surface with water for a period of time before freezing it in liquid nitrogen to image the surface. By varying the time the surface is covered in water, it would be possible to image the evolution of the surface during restructuring.

The mechanical properties of the hydrogels in this study were analyzed while changing only two variables: the alginate concentration and the pH of the formulation. These are certainly not the only the parameter which can change the mechanical properties of these materials. Since the interactions between gelatin and alginate are likely mostly electrostatic another important variable could be the ionic strength of the materials.[30] Increasing the ionic strength of the samples would reduce the strength of the electrostatic interactions by screening charges on neighboring chains. The samples used in this report were prepared with DI water and were not buffered, nor were any additional ions added (except those used for pH adjustment). This would

allow the chains to interact to the greatest extent possible, and it is expected that increasing ionic strength would decrease the mechanical properties of both the neat and blend samples. Furthermore, since alginate is present in the system, divalent and monovalent ions will have vastly different impacts on final mechanical properties. Future work in this area may include carefully measuring the ion content of the raw gelatin powder and may require additional purification to remove or reduce the amount of calcium present in the gelatin.

LIST OF REFERENCES

1. Veis, A., *The macromolecular chemistry of gelatin.* Academic Press: New York, 1964.
2. Djabourov, M.; Leblond, J.; Papon, P., GELATION OF AQUEOUS GELATIN SOLUTIONS .1. STRUCTURAL INVESTIGATION. *Journal De Physique* **1988,** *49* (2), 319-332.
3. America, G. M. I. o., Gelatin Handbook. 2012.
4. Keenan, T. R., Gelatin. In *Kirk-Othmer Encyclopedia of Chemical Technology*, John Wiley & Sons, Inc.: 2000.
5. Duconseille, A.; Astruc, T.; Quintana, N.; Meersman, F.; Sante-Lhoutellier, V., Gelatin structure and composition linked to hard capsule dissolution: A review. *Food Hydrocolloids* **2015,** *43*, 360-376.
6. Araki, K.; Ozeki, T., Amino Acids. In *Kirk-Othmer Encyclopedia of Chemical Technology*, John Wiley & Sons, Inc.: 2000.
7. Bigi, A.; Cojazzi, G.; Panzavolta, S.; Roveri, N.; Rubini, K., Stabilization of gelatin films by crosslinking with genipin. *Biomaterials* **2002,** *23* (24), 4827-4832.
8. Bigi, A.; Panzavolta, S.; Rubini, K., Relationship between triple-helix content and mechanical properties of gelatin films. *Biomaterials* **2004,** *25* (25), 5675-5680.
9. Saarai, A.; Kasparkova, V.; Sedlacek, T.; Saha, P., On the development and characterisation of crosslinked sodium alginate/gelatine hydrogels. *Journal of the Mechanical Behavior of Biomedical Materials* **2013,** *18*, 152-166.
10. Xing, Q.; Yates, K.; Vogt, C.; Qian, Z. C.; Frost, M. C.; Zhao, F., Increasing Mechanical Strength of Gelatin Hydrogels by Divalent Metal Ion Removal. *Scientific Reports* **2014,** *4*, 10.
11. Dong, Z. F.; Wang, Q.; Du, Y. M., Alginate/gelatin blend films and their properties for drug controlled release. *Journal of Membrane Science* **2006,** *280* (1-2), 37-44.
12. Yang, Y.; Anvari, M.; Pan, C. H.; Chung, D., Characterisation of interactions between fish gelatin and gum arabic in aqueous solutions. *Food Chemistry* **2012,** *135* (2), 555-561.
13. Cote, G. L.; Ahlgren, J. A., Microbial Polysaccharides. In *Kirk-Othmer Encyclopedia of Chemical Technology*, John Wiley & Sons, Inc.: 2000.
14. Draget, K. I.; Braek, G. S.; Smidsrod, O., ALGINIC ACID GELS - THE EFFECT OF ALGINATE CHEMICAL-COMPOSITION AND MOLECULAR-WEIGHT. *Carbohydrate Polymers* **1994,** *25* (1), 31-38.
15. Hoffman, A. S., Hydrogels for biomedical applications. *Advanced Drug Delivery Reviews* **2002,** *54* (1), 3-12.
16. Papageorgiou, H.; Kasapis, S.; Gothard, M. G., STRUCTURAL AND TEXTURAL PROPERTIES OF CALCIUM-INDUCED, HOT-MADE ALGINATE GELS. *Carbohydrate Polymers* **1994,** *24* (3), 199-207.

17. Wang, Z. Y.; Zhang, Q. Z.; Konno, M.; Saito, S., SOL-GEL TRANSITION OF ALGINATE SOLUTION BY THE ADDITION OF VARIOUS DIVALENT-CATIONS - C-13-NMR SPECTROSCOPIC STUDY. *Biopolymers* **1993,** *33* (4), 703-711.

18. Lu, L.; Liu, X. X.; Qian, L. Y.; Tong, Z., Sol-gel transition in aqueous alginate solutions induced by cupric cations observed with viscoelasticity. *Polymer Journal* **2003,** *35* (10), 804-809.

19. Liu, X. X.; Qian, L. Y.; Shu, T.; Tong, Z., Rheology characterization of sol-gel transition in aqueous alginate solutions induced by calcium cations through in situ release. *Polymer* **2003,** *44* (2), 407-412.

20. Grasdalen, H.; Larsen, B.; Smidsrod, O., PMR STUDY OF THE COMPOSITION AND SEQUENCE OF URONATE RESIDUES IN ALGINATES. *Carbohydrate Research* **1979,** *68* (1), 23-31.

21. Grasdalen, H., HIGH-FIELD, H-1-NMR SPECTROSCOPY OF ALGINATE - SEQUENTIAL STRUCTURE AND LINKAGE CONFORMATIONS. *Carbohydrate Research* **1983,** *118* (JUL), 255-260.

22. Boateng, J. S.; Matthews, K. H.; Stevens, H. N. E.; Eccleston, G. M., Wound healing dressings and drug delivery systems: A review. *Journal of Pharmaceutical Sciences* **2008,** *97* (8), 2892-2923.

23. Lee, H. J.; Ahn, S. H.; Kim, G. H., Three-Dimensional Collagen/Alginate Hybrid Scaffolds Functionalized with a Drug Delivery System (DDS) for Bone Tissue Regeneration. *Chemistry of Materials* **2012,** *24* (5), 881-891.

24. Sisney, G. A.; Hunt, K. A., A low-cost gelatin phantom for learning sonographically guided interventional breast radiology techniques. *American Journal of Roentgenology* **1998,** *171* (1), 65-66.

25. Young, S.; Wong, M.; Tabata, Y.; Mikos, A. G., Gelatin as a delivery vehicle for the controlled release of bioactive molecules. *Journal of Controlled Release* **2005,** *109* (1-3), 256-274.

26. Sridhar, M.; Liu, J.; Insana, M. F., Elasticity imaging of polymeric media. *Journal of Biomechanical Engineering-Transactions of the Asme* **2007,** *129* (2), 259-272.

27. Yapp, R. D.; Kalyanam, S.; Insana, M. F. In *Molecular and structural analysis of viscoelastic properties*, 2007; pp 65111Y-65111Y-11.

28. Yapp, R. D.; Insana, M. F., pH-induced contrast in viscoelasticity imaging of biopolymers. *Physics in Medicine and Biology* **2009,** *54* (5), 1089-1109.

29. Xiao, C. B.; Liu, H. J.; Lu, Y. S.; Zhang, L., Blend films from sodium alginate and gelatin solutions. *Journal of Macromolecular Science-Pure and Applied Chemistry* **2001,** *38* (3), 317-328.

30. Razzak, M. A.; Kim, M.; Chung, D., Elucidation of aqueous interactions between fish gelatin and sodium alginate. *Carbohydrate Polymers* **2016,** *148*, 181-188.

31. Deng, C. M.; He, L. Z.; Zhao, M.; Yang, D.; Liu, Y., Biological properties of the chitosan-gelatin sponge wound dressing. *Carbohydrate Polymers* **2007,** *69* (3), 583-589.

32. Liu, L. S.; Liu, C. K.; Fishman, M. L.; Hicks, K. B., Composite films from pectin and fish skin gelatin or soybean flour protein. *Journal of Agricultural and Food Chemistry* **2007,** *55* (6), 2349-2355.

33. Chen, Y. X.; Cain, B.; Soman, P., Gelatin methacrylate-alginate hydrogel with tunable viscoelastic properties. *Aims Materials Science* **2017,** *4* (2), 363-369.

34. Goudoulas, T. B.; Germann, N., Phase transition kinetics and rheology of gelatin-alginate mixtures. *Food Hydrocolloids* **2017,** *66*, 49-60.

35. Zhang, H. M.; Wang, Y.; Insana, M. F., Ramp-hold relaxation solutions for the KVFD model applied to soft viscoelastic media. *Measurement Science and Technology* **2016,** *27* (2), 11.

36. Lakes, R. S., *Viscoelastic Solids*. Taylor & Francis: 1998.

37. Magin, R. L., Fractional calculus in bioengineering. Begell House Redding: 2006.

38. Torvik, P. J.; Bagley, R. L., ON THE APPEARANCE OF THE FRACTIONAL DERIVATIVE IN THE BEHAVIOR OF REAL MATERIALS. *Journal of Applied Mechanics-Transactions of the Asme* **1984,** *51* (2), 294-298.

39. Koeller, R. C., APPLICATIONS OF FRACTIONAL CALCULUS TO THE THEORY OF VISCOELASTICITY. *Journal of Applied Mechanics-Transactions of the Asme* **1984,** *51* (2), 299-307.

40. Mainardi, F.; Spada, G., Creep, relaxation and viscosity properties for basic fractional models in rheology. *European Physical Journal-Special Topics* **2011,** *193* (1), 133-160.

41. Sigma-Aldrich Gelatins - Product Information Sheet. https://www.sigmaaldrich.com/content/dam/sigma-aldrich/docs/Sigma/Product_Information_Sheet/2/g9382pis.pdf (accessed May 30, 2017).

42. Sigma-Aldrich Alginic acid sodium salt. https://www.sigmaaldrich.com/catalog/product/aldrich/180947?lang=en&region=US (accessed May 30, 2017).

43. Sun, J. Y.; Zhao, X. H.; Illeperuma, W. R. K.; Chaudhuri, O.; Oh, K. H.; Mooney, D. J.; Vlassak, J. J.; Suo, Z. G., Highly stretchable and tough hydrogels. *Nature* **2012,** *489* (7414), 133-136.

44. Hatakeyama, H.; Hatakeyama, T., Interaction between water and hydrophilic polymers. *Thermochimica Acta* **1998,** *308* (1-2), 3-22.

45. Ping, Z. H.; Nguyen, Q. T.; Chen, S. M.; Zhou, J. Q.; Ding, Y. D., States of water in different hydrophilic polymers - DSC and FTIR studies. *Polymer* **2001,** *42* (20), 8461-8467.

46. Djabourov, M.; Leblond, J.; Papon, P., GELATION OF AQUEOUS GELATIN SOLUTIONS .2. RHEOLOGY OF THE SOL-GEL TRANSITION. *Journal De Physique* **1988,** *49* (2), 333-343.

47. Cumper, C. W. N.; Alexander, A. E., THE VISCOSITY AND RIGIDITY OF GELATIN IN CONCENTRATED AQUEOUS SYSTEMS .2. RIGIDITY. *Australian Journal of Scientific Research Series a-Physical Sciences* **1952,** *5* (1), 153-159.

48. Altahhan, K. N.; Wang, Y.; Sobh, N.; Insana, M. F., Indentation Measurements to Validate Dynamic Elasticity Imaging Methods. *Ultrasonic Imaging* **2016,** *38* (5), 332-345.

49. Toohey, K. S.; Kalyanam, S.; Palaniappan, J.; Insana, M. F., Indentation analysis of biphasic viscoelastic hydrogels. *Mechanics of Materials* **2016,** *92*, 175-184.

50. Bialopiotrowicz, T.; Janczuk, B., Surface properties of gelatin films. *Langmuir* **2002,** *18* (24), 9462-9468.

51. Holly, F. J., WETTABILITY OF HYDROGELS .1. POLY(2-HYDROXYETHYL METHACRYLATE). *Journal of Biomedical Materials Research* **1975,** *9* (3), 315-326.

52. Lewis, W. K.; Squires, L.; Broughton, G., *Industrial Chemistry of Colloidal and Amorphous Materials*. Macmillan: 1942.

53. Loeb, J., *Proteins and the Theory of Colloidal Behavior*. McGraw-Hill Book Company, Incorporated: 1922.

54. Saarai, A.; Sedlacek, T.; Kasparkova, V.; Kitano, T.; Saha, P., On the characterization of sodium alginate/gelatine-based hydrogels for wound dressing. *Journal of Applied Polymer Science* **2012,** *126*, E79-E88.

55. Muyonga, J. H.; Cole, C. G. B.; Duodu, K. G., Fourier transform infrared (FTIR) spectroscopic study of acid soluble collagen and gelatin from skins and bones of young and adult Nile perch (Lates niloticus). *Food Chemistry* **2004,** *86* (3), 325-332.

56. Al-Saidi, G. S.; Al-Alawi, A.; Rahman, M. S.; Guizani, N., Fourier transform infrared (FTIR) spectroscopic study of extracted gelatin from shaari (Lithrinus microdon) skin: effects of extraction conditions. *International Food Research Journal* **2012,** *19* (3), 1167-1173.

57. Li, Y. F.; Jia, H. P.; Cheng, Q. L.; Pan, F. S.; Jiang, Z. Y., Sodium alginate-gelatin polyelectrolyte complex membranes with both high water vapor permeance and high permselectivity. *Journal of Membrane Science* **2011,** *375* (1-2), 304-312.

58. Hashim, D. M.; Man, Y. B. C.; Norakasha, R.; Shuhaimi, M.; Salmah, Y.; Syahariza, Z. A., Potential use of Fourier transform infrared spectroscopy for differentiation of bovine and porcine gelatins. *Food Chemistry* **2010,** *118* (3), 856-860.

59. Nguyen, T.; Lee, B., Fabrication and characterization of cross-linked gelatin electro-spun nano-fibers. *Journal of Biomedical Science and Engineering* **2010,** (3), 1117-1124.

APPENDIX A: Analysis of ATR FTIR spectra

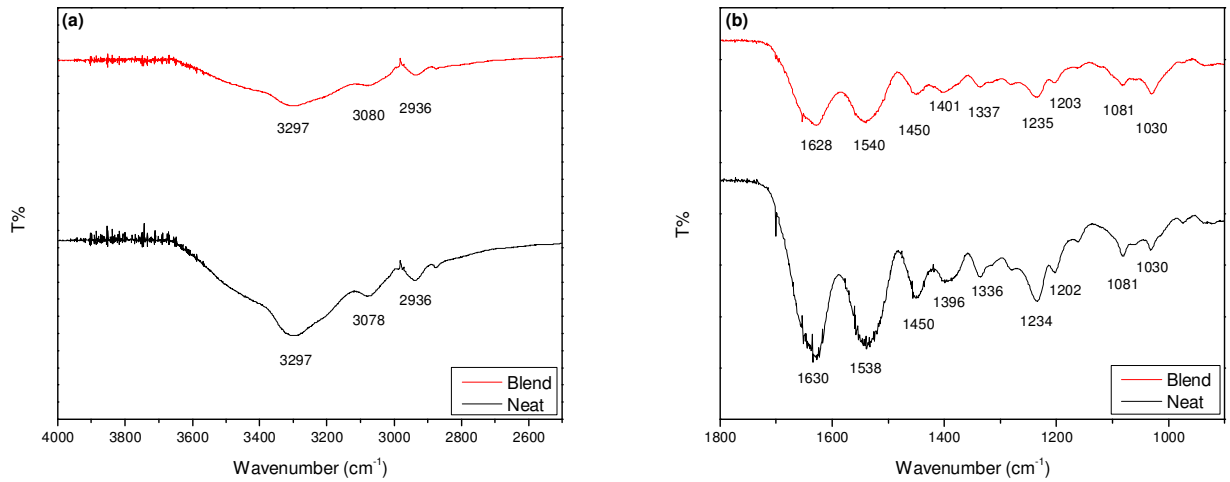

Figure 20. IR spectra of 5% w/w gelatin (black) and 5/1% w/w blend (red) films over the range (a) 2500 – 4000 cm^{-1} and (b) 900 – 1800 cm^{-1}.

The IR spectrum of gelatin and gelatin/alginate blends has been extensively studied.[9-11, 29, 54-59] The characteristic peaks of the gelatin spectrum occur at 1620 – 1660 cm^{-1} (C=O stretch), 1520 – 1550 cm^{-1} (N-H bend and C-H stretch), and 1230 – 1240 cm^{-1} (C-N stretch and N-H bend). These peaks are commonly referred to as Amide I, Amide II, and Amide III, respectively. Additionally, a broad peak around 3300 cm^{-1} corresponds to N-H bond stretching of amide groups participating in hydrogen bonding (Amide A), and the shoulder on this peak may be due to O-H stretching due to water in the film. Sodium alginate has characteristic peaks at 1411 cm^{-1} (COO^- symmetric stretch), 1080 cm^{-1} (C-O stretch), 1030 cm^{-1} (CO-C stretch), and around 3300 cm^{-1} corresponding to hydroxyl stretching.

As mentioned earlier, the strength of gelatin hydrogels is directly related to intermolecular interactions between neighboring gelatin chains. In the IR spectrum of gelatin, others have reported previously that increased intermolecular interactions can be associated with a shift in the Amide I, II, and III peaks to lower wavenumbers. From Figure 20b, it does not appear that any of these peaks experience a significant shift on the addition of alginate. This

could indicate that alginate does not have a significant effect on the intermolecular interactions between gelatin molecules. Other studies on the IR spectra of gelatin have found that the Amide I peak is associated with the random coil conformation of gelatin and the Amide III peak is associated with the triple helix conformation.[55, 56, 58] The ratio of the intensity of the Amide I and Amide III peaks can then be used to determine the helix content in the cured films. There is no difference in the ratio of these two peaks based on their peak absorbances, which indicates the same helix content between the two films. The O-H and N-H stretching peaks at around 3300 cm^{-1} are broad because they are associated with hydrogen bonds of varying strengths. It is generally accepted that the lowest wavenumber in this band can be attributed to the strongest hydrogen bonds, such as those between charged groups and water in the first hydration layer. An increase in hydrogen bonding would, therefore, cause a shift in this peak to lower wavenumbers. This shift is not seen in Figure 20a.

The only major differences between the IR spectra of the neat and blend samples is a shift of the peak at 1396 cm^{-1} to higher wavenumbers on the addition of alginate and an increase in the intensity of the C-O stretching peak at 1081 cm^{-1}. Sodium alginate has peaks around 1411 cm^{-1} and 1080 cm^{-1} so it is likely both of these changes are simply due to the addition of these peaks to the native gelatin spectrum, and not due to changes in intermolecular interactions.

APPENDIX B: Alginate network formation via native Ca^{2+} ions in gelatin

Raw gelatin powder contains a number of trace elements such as sodium, calcium, and potassium.[3] The concentrations of these impurities vary based on the specific manufacturing method. Since gelatin/alginate interactions are predominately electrostatic, even the small ionic contribution from manufacturing may be important to the final mechanical properties of the blend samples. Furthermore, sodium alginate has the potential to "scavenge" calcium ions from solution to form a calcium alginate network.

Liu et al. has previously studied the rheological characteristics of 3% w/w sodium alginate solutions in the presence of calcium cations.[19] Specifically, they looked into the effect of calcium ion concentration on the viscoelastic properties around the critical calcium concentration. This critical concentration is the point where a gel of infinite molecular weight just barely begins to form. At this point, the tangent of the loss angle is independent of frequency. The group defined a parameter, f, as:

$$f = \frac{[Ca^{2+}]}{[COO^{-}\ in\ alginate]} \tag{18}$$

In alginate, the two primary factors controlling the formation of a gel network are the molecular weight and the ratio of mannuronic acid to guluronic acid residues in the chains. Since only guluronic acid has the buckled geometry necessary to form an egg-box junction with neighboring alginate chains, alginate which contain more guluronic acid will form stronger gels. The definition of f given above does not differentiate between COO^- groups on guluronate versus mannuronate, so it is not obvious whether an alginate containing more guluronate will have a higher or lower critical calcium concentration, f_c, than one containing more mannuronate.

The following few paragraphs will go through the calculations to determine the value of f for the system used in this report.

On average, Type B gelatin contains around 900 ppm of calcium.[3] The calcium concentration in the first batch of gelatin mentioned in this report was determined by titration to be around 800 ppm which was close enough to the literature to use a value of 900 ppm for the following calculations. Assuming a basis of 100 g of solution, a 5% w/w gelatin solution would then contain 0.0045 g of calcium. If the density of this solution is approximately 1 g/cm^3 the resulting Ca^{2+} concentration is 1.12 mM.

Sigma-Aldrich provided an estimate for the sodium alginate molecular weight of approximately 155,000 g/mol.[42] Both mannuronate and guluronate have a molecular weight of 194.14 g/mol, so there are around 798 residues in each alginate chain. Since the pKa values of mannuronic acid and guluronic acid residues are 3.38 and 3.65, respectively, it was assumed that at the pH range studied every carboxylic acid was deprotonated and therefore each alginate chain contributes 798 COO^- groups. Again assuming a basis of 100 g of solution, a 1% w/w alginate solution would contain 1 g of alginate. Using the molecular weight for alginate above the resulting COO^- concentration is 51.5 mM.

Using equation 18, the resulting value of f is 0.022. Liu et al. found that f_c was approximately 0.04. Furthermore, in calculating the value of f above it was assumed that every Ca^{2+} ion present in solution migrated to the alginate chains and that gelatin did not exist beyond its Ca^{2+} contribution. In reality, gelatin also contains many COO^- groups which would also attract calcium ions and electrostatic interactions between positively charged groups on gelatin may interfere with the formation of egg-box junctions in alginate. Therefore, the calculated value of f represents a true best-case scenario and it is still short of the predicted critical ion

concentration. Since this value is greater than the value of the 5/1% w/w gelatin/alginate solution used throughout the majority of this report, it is unlikely a calcium alginate gel network is present in these samples. Despite there not being enough Ca^{2+} present in solution to form a complete gel network, crosslinking may still occur to a significant enough extent to form a viscoelastic fluid.

Since every sample used in this report contained 5% w/w gelatin, the Ca^{2+} concentration is constant and by repeating the calculations above in reverse, the maximum amount of alginate which can be crosslinked to form a critical gel can be calculated. Once again making the assumptions stated in the last paragraph, this alginate concentration was found to be approximately 0.5% w/w, with the value of f increasing with decreasing alginate concentration. As mentioned in Section 3.1, Figure 6b showed a statistically significant increase in the elastic modulus at the lowest alginate concentration. At this concentration, the predicted value of f is greater than f_c and the formation of a calcium alginate gel network may be possible and could explain the increase in elastic modulus. However, it may be impossible to check the validity of the assumption highlighted above.

ROSE-HULMAN INSTITUTE OF TECHNOLOGY

Final Examination Report

Michael A. Samp — Name

Chemical Engineering — Graduate Major

Thesis Title: Sodium Alginate Toughening of Gelatin Hydrogels and Elucidation of Possible Mechanisms

DATE OF EXAM: July 11, 2017

EXAMINATION COMMITTEE:

	Thesis Advisory Committee	Department
Thesis Advisor:	David Henthorn, Co-Advisor	CHE
	Adam Nolte, Co-Advisor	CHE
	Mark Brandt	CHEM

PASSED X **FAILED**